# Modeling and Design Optimization of Plug-In Hybrid Electric Vehicle Powertrains

by

Maryyeh Chehresaz

A thesis
presented to the University of Waterloo
in fulfillment of the
thesis requirement for the degree of
Master of Applied Science
in
Systems Design Engineering

Waterloo, Ontario, Canada, 2013

I hereby declare that I am the sole author of this thesis. This is a true copy of the thesis, including any required final revisions, as accepted by my examiners.

I understand that my thesis may be made electronically available to the public.

## Abstract

Hybrid electric vehicles (HEVs) were introduced in response to rising environmental challenges facing the automotive sector. HEVs combine the benefits of electric vehicles and conventional internal combustion engine vehicles, integrating an electrical system (a battery and an electric motor) with an engine to provide improved fuel economy and reduced emissions, while maintaining adequate driving range. By comparison with conventional HEVs, plug-in hybrid electric vehicles (PHEVs) have larger battery storage systems and can be fully charged via an external electric power source such as the electrical grid. Of the three primary PHEV architectures, power-split architectures tend to provide greater efficiencies than parallel or series systems; however, they also demonstrate more complicated dynamics. Thus, in this research project, the problem of optimizing the component sizes of a power-split PHEV was addressed in an effort to exploit the flexibility of this powertrain system and further improve the vehicle's fuel economy, using a Toyota plug-in Prius as the baseline vehicle. Autonomie software was used to develop a vehicle model, which was then applied to formulate an optimization problem for which the main objective is to minimize fuel consumption over standard driving cycles. The design variables considered were: the engine's maximum power, the number of battery cells and the electric motor's maximum power. The genetic algorithm approach was employed to solve the optimization problem for various drive cycles and an acceptable reduction in fuel consumption was achieved thorough the sizing process. The model was validated against a MapleSim model.

This research project successfully delivered a framework that integrates an Autonomie PHEV model and genetic algorithm optimization and can be used to address any HEV parameter optimization problem, with any objective, constraints, design variables and optimization parameters.

**Acknowledgements**

I would like to thank my supervisor, Professor Nasser Azad for his tremendous support, encouragement and guidance.

I am also grateful to Professor John McPhee and Professor Andrea Scott for providing constructive suggestions and valuable comments on my thesis.

My work would not been successful without the guidance and help of my friends and labmates, Mahyar, Reza, Naser and Mehdi. I express my heartfelt thanks to all of them. It was a pleasant experience to work with them in such a wonderful and vivid environment.

I express my deep sense of gratitude to my parents for their love, support and prayers throughout my life.

*To My Parents*

# Table of Contents

# List of Tables

# List of Figures

# Chapter 1

# Introduction

## 1.1 Background

Dwindling natural resources, such as oil and gas, as well as noise and toxic tailpipe emissions have been major concerns in the automotive sector for decades. Vehicle manufacturers have been under constant pressure to address these problems through new, lower fuel consumption, lower emissions vehicle platforms.

### 1.1.1 Electric Vehicles

Electric Vehicles (EVs) were introduced as a viable solution to noisy, gas guzzling internal combustion engine (ICE) vehicles. Relying exclusively on electrical energy from the battery system for power, EVs completely eliminate the need for direct fossil-fuel consumption and produce no noise or tailpipe emissions. However, despite these advantages, EVs have not

made a significant impact on global vehicle markets, where conventional ICE vehicles continue to dominate. This is largely due to the high cost and limited electric range of electric vehicles.

Consequently, as vehicle manufacturers work to address these drawbacks, they have also had to introduce platforms that can effectively bridge the gap between ICE and zero-emissions vehicles, serving as transition technologies until EVs can more deeply penetrate the consumer market. This effort has resulted in hybrid electric, and later plug-in hybrid electric, vehicles (HEVs and PHEVs, respectively).

### 1.1.2 Hybrid Electric Vehicles

As mentioned previously, the HEV was presented as a transitory solution that takes advantage of technologies from both EV and ICE platforms by integrating electric motors from the EV with the internal combustion engine of conventional vehicles, providing an alternative source of energy for vehicle propulsion. Therefore, HEVs are more efficient than conventional vehicles because the electric system helps the engine stay within its most efficient operating range, allowing it to charge the batteries with excess power or turn off during idling time. This is particularly useful in urban areas, where the electric system can be used almost exclusively to drive the vehicle, allowing for a smaller engine and leading to lower fuel consumption. Furthermore, energy typically wasted during braking can be recaptured and used to charge the batteries. All of these advantages are helpful to achieve a better fuel economy. However, while HEVs cannot run on the electric system alone, and therefore must consume at least a small amount of fuel, they can be considered a feasible

mid-term solution until zero-fuel consumption, zero-emissions EVs are fully realized

### 1.1.3 Plug-in Hybrid Electric Vehicles

PHEVs are essentially HEVs that can connect to the electrical grid and store electric energy using rechargeable batteries. PHEVs have larger battery capacities than HEVs and as a result offer an extended electric range. Therefore, PHEVs offer combined advantages of HEVs and EVs, making them the best solution on the market today.

### 1.1.4 Powertrain Configurations

HEVs and PHEVs have four main components, including: an ICE, an electric motor, a generator and a battery pack. These components can be connected to each other in many different ways; however, the three configurations typically seen in HEVs/PHEVs are series, parallel, and power-split.

In series architecture 1.1, the generator and battery are connected to the electric motor, which propels the vehicle alone. The ICE in this architecture is coupled with the generator to charge the battery or provide power to the electric motor. Series configuration is more efficient at lower speeds and therefore it is appropriate for urban driving.

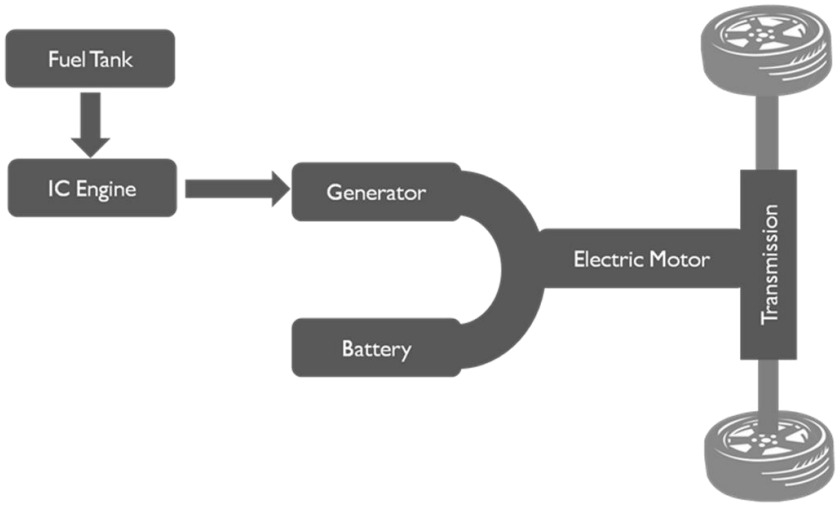


Figure 1.1: Series configuration

Parallel architectures 1.2 connect both the ICE and electric motor to the transmission, which can simultaneously drive the wheels. Thus, this configuration is appropriate for higher speeds and highway driving.

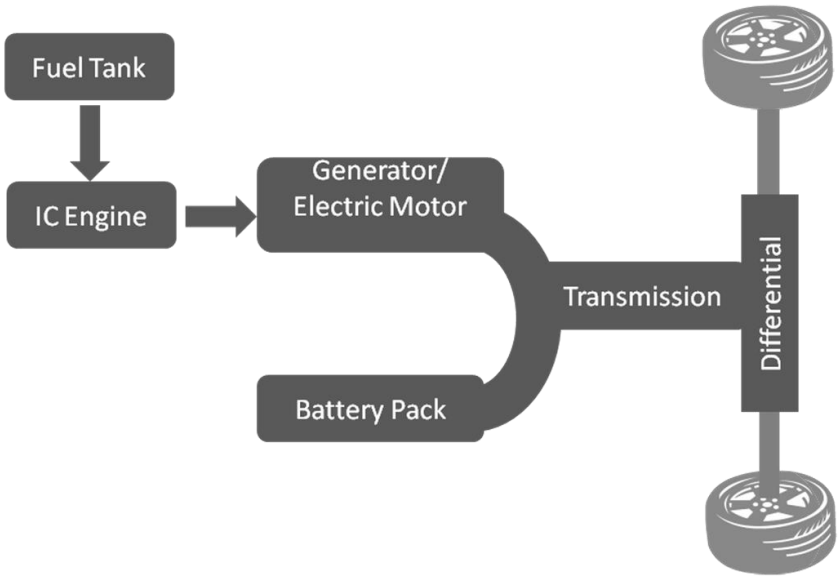


Figure 1.2: Parallel configuration

The power-split configuration 1.3 combines benefits from series and parallel architectures, offering the most efficient option, but the most complicated design. It includes a planetary gear as the transmission where the electric motor, generator and ICE connect to the ring, sun and carrier gears, respectively.

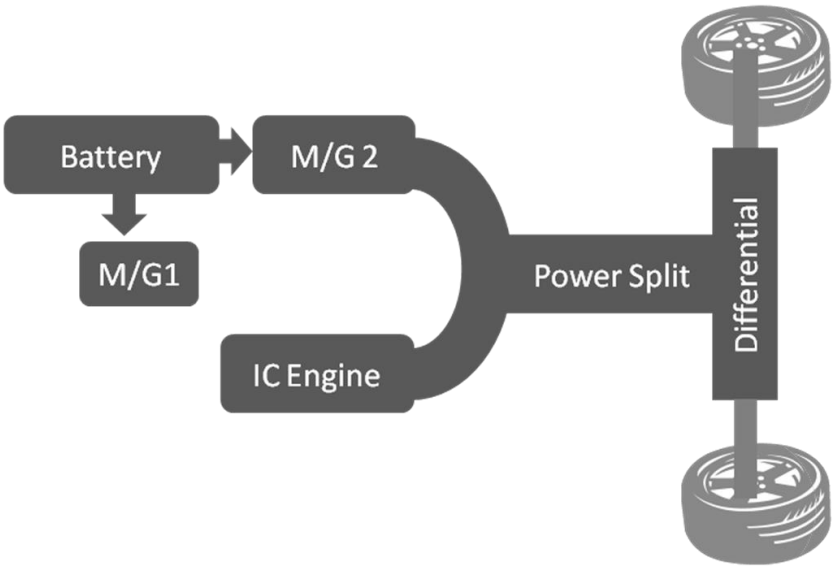


Figure 1.3: Power-split configuration

## 1.2 Objective

Rising environmental concerns have forced governments all around the world to establish new and very ambitious regulations that will see vehicles produced with improved fuel economy and lower emissions in the near-term. These regulations, such as the CAFE (Corporate Average Fuel Economy) in the USA or those enacted by the European Economic Committee, obligate manufacturers to pay steep penalties if the average fuel economy of their products fall below the limits defined by these standards. Therefore, automotive manufacturers are under constant pressure to reduce the fuel consumption of their vehicle fleets. EV technologies are good solutions for these standards but have significant drawbacks that limit their appeal to consumers, namely cost and driving range. Thus, finding

alternative ways to minimize fuel consumption is always an essential objective for automotive researchers and manufacturers. Consequently, this study attempted to minimize the fuel consumption in a PHEV, specifically the Toyota plug-in Prius, as much as possible.

There are various ways to achieve this goal. One possible approach, and the one taken here, is to size the main components of the PHEV in a way that minimizes fuel consumption while maintaining acceptable vehicle performance. A vehicle model and an optimization algorithm are prerequisites for optimizing the size of components.

For modeling, a simulation tool is required. In this work, Autonomie, which is a Matlab-based vehicle simulator, was used and a model of a PHEV with Toyota Prius characteristics was developed.

Many algorithms are available to support optimization. The most prominent in the sizing of HEV/PHEV components are global optimization algorithms, such as Genetic Algorithm (GA), Particle Swarm Optimization (PSO), and Dynamic Programming (DP). Gradient- based methods have also been integrated with global methods to provide a robust sizing algorithm, which takes advantage of benefits from both methods and minimizes the drawbacks.

Optimization can be carried out with respect to a single or multiple objectives. In general, the most important objectives to HEV/PHEV component sizing are cost, weight of the vehicle, emissions and fuel consumption.

Therefore, equipped with a PHEV model in one hand and an optimization algorithm in the other, our aim in this study was to find the optimized sizing for powertrain components with the objective of minimizing fuel consumption. As a result, we have created

a framework that integrates a high-fidelity model and optimization technique and can be used to address a broad range of objectives, design variables and constraints.

## 1.3 Outline

The contents of this thesis are organized into five chapters. Following the brief introduction to hybrid vehicles and general purpose of this study provided in this chapter, Chapter 2 provides a review of the literature related to the modeling and sizing optimization of HEV/PHEVs. In Chapter 3, the modeling of a PHEV with Toyota Prius characteristics is described, and an evaluation of the developed model is presented to consider the impact of different components on the fuel economy. In Chapter 4, the sizing of the powertrain components is carried out by employing GA. Finally, Chapter 5 outlines the overall conclusions that can be derived from this study.

# Chapter 2

# Literature Review

Environmental concerns have become the primary drivers behind technological advancement in the automotive manufacturing sector, and have subsequently spurred development of HEVs/PHEVs. As described in Chapter 1, HEVs are complex electro-mechanical systems involving hundreds of design parameters. Thus, to achieve better HEV performance, each parameter must be carefully chosen at the design stage. Since prototyping and testing each design combination is expensive and time consuming, optimization algorithms and simulation techniques, which reduce validation activities, are critical to achieving optimized component sizing at minimal cost.

This chapter presents recent work on the modeling, sizing and design optimization of HEVs/PHEVs.

## 2.1 Powertrain Modeling

This section provides insights and outlines upcoming challenges related to the modeling of HEVs/PHEVs.

Depending on the level of detail required, different techniques of physics-based dynamic modeling or empirical modeling (using look-up tables or maps) can feasibly be applied to develop an HEV or PHEV model. However, a trade off exists between the fidelity and run-time of a model, where higher fidelity models, which more accurately represent the behaviour of a system, typically require more time for computation and simulation. That being said, a model should always be built with sufficient fidelity to address the desired application and objective. For instance, the evaluation of a control strategy requires a model with higher fidelity and detail.

Golbuff [1] developed a parallel PHEV model in PSAT (Powertrain System Analysis Toolkit) for optimization purposes (primarily cost). A mid-sized sedan was used as a baseline vehicle platform and specific vehicle components were integrated on it. Most of the components in PSAT use look-up tables within their subsystems. The data for these components models were measured and compiled at Argonne National Laboratory (ANL) and are included with PSAT. Zeman et al. [2] modeled different PHEV architectures (series, power-split,...) to compare fuel economies and find optimized control strategies. GT-SUITE, a multi-physics CAE (Computer Aided Engineering) platform for engine and vehicle simulation supported this effort. More specifically, Zeman's group exploited look-up tables and maps to model the engine, electric motors and battery. Moreover, all the control strategies were modeled using this tool as well.

As a case for mathematics-based modeling, Dao et al. [3] used MapleSim, a physical modeling tool developed by Maplesoft Inc., to develop a high fidelity model of a series HEV for real-time applications, such as HIL (hardware-in-the-loop) simulations or to investigate vehicle performance. Utilizing a mean-value engine, a chemistry-based battery and a 3D multibody vehicle model have given a higher fidelity to the proposed symbolic model. In most cases, physic-based and empirical modeling are considered together. Mapelli et al. [4] and Cheli et al. [5] used Matlab/Simulink to model a PHEV and built a prototype to experimentally validate their model. The VolksWagen Crafter was used as a base vehicle platform and hybridized by adding and installing an electrical drive system. The validated model was used for further analysis, design and control. In different driving modes, simulations were carried out with the objective of reducing emissions. To model the main components, a math-based model was used to address the electric motor while maps were used to model the engine and battery.

In another example that combines maps and physics-based models, Zhumu et al. [6] modeled a parallel HEV using Advisor. They established the main powertrain models by combining experimental and mathematical modeling. The performance of their simulated models were verified by comparing the results with Santana 2000GLi.

HEV modeling involves a variety of different physical domains, such as mechanical [7,8] electrical [9, 10], and thermal [9, 11–14]. Within the collective body of HEV/PHEV modeling and simulation research, only a few studies have addressed multi-domain modeling of HEVs [3, 6, 12, 15, 16]or PHEVs [1, 2, 4, 5] as an entire vehicle system, while other works have produced high fidelity models of specific powertrain components, such as the electric motor [5] or battery pack [13, 14, 17, 18]. In addition to this category and based on

the physical domain, models have been developed for parallel [2, 6, 19, 20], series [2, 3] and power-split [7, 21] configurations as well.

Models can be categorized as steady state, quasi-static, or transient [22]. By comparison with steady-state models, transient models include more details and dynamics information for the components considered, while quasi-static models fall somewhere between these two. Fully detailed transient modeling is primarily used in real-time and HIL simulation, which requires more time for computation.

From another perspective, models can be divided into backward and forward categories. A backward model takes the driving cycle as the input and assumes the model tracks it exactly. Therefore, the vehicle speed is assumed to be known and the model calculates the demanded power. Steady-state models usually take advantage of backward modeling [22]. Backward modeling is an ideal method for component sizing purposes due to its simplicity and low computation time. Forward modeling attempts to simulate real world driving and therefore requires more simulation time. These models take acceleration and braking commands from the driver as input and give the vehicle performance as output. Musardo et al. [23] used a forward quasi-static model in their studies because it is more appropriate for control strategy development.

It can be concluded that [4, 5, 16, 24] many of the tools and simulation packages developed for vehicle powertrain modeling take advantage of the Matlab/Simulink environment. ADVISOR, V-Elph, MapleSim, PSAT, and Autonomie are some other modeling simulators used on the market. Each provides a user-friendly environment.

Butler et al. [16] developed a simulation and modeling package for HEV and PHEV

design called V-Elph. V-Elph, which is based on Matlab/Simulink, consists of detailed powertrain components models that can be integrated together to make different configurations.

Taking advantage of model-based development processes, Che et al. [25] employed VMA (Vehicle Model Architecture) to develop a Dual Drive HEV model for model-in-the-loop (MIL) and hardware-in-the-loop (HIL) applications. The VMA was based on a Ford-internal architecture, which was subsequently modified and released as the Vehicle Interfaces library [26]. The system described in this work has two mechanical drive paths in EV and parallel operating modes. A dynamic model of the gear box was built in Dymola, which was later integrated into VMA to create a vehicle system as well as a component level subsystem. This vehicle model mainly utilizes a mean-value engine and dual clutch transmission models.

In another effort, a dynamic Graphical User Interface vehicle model was developed for PHEVs using Matlab [24]. This tool provides users with the option of selecting vehicle and driving conditions in manual or automatic modes. Models for each component of a series-parallel HEV were developed based on dynamic principles and simulated for four Toyota hybrid platforms [24].

Consequently, work done in the modeling of HEV/PHEV can be categorized in terms of what simulation tool has been used, what type of architecture was addressed or which components were modeled. However, in terms of model fidelity, it can be concluded that the trend is toward developing models that contain enough information and detail, but also do not require lengthy simulation times. Graphical user interface simulation tools ease this

process.

## 2.2 Powertrain Component Sizing Methodology

Efforts to optimize HEV/PHEV component sizing are summarized here. Work done in this field can be classified according to the components considered, objectives pursued, optimization methods used, configurations addressed, and type of drive cycle selected.

### 2.2.1 Powertrain Configurations

As explained in the previous chapter, among the three main HEV/PHEV powertrain configurations, the power-split architecture is recognized as the most feasible configuration to significantly improve fuel economy and emissions [27]. Sizing methodology utilizing a power-split configuration was investigated in [27–29]. Series and parallel architectures have also been considered; for example, Hasanzadeh et al. [30] provides the optimum design of a diesel engine for a hybrid series bus and for a particular driving cycle, whereas Wu et al. [31] attempted to improve fuel consumption in a parallel HEV. Multi-objective sizing optimization of a parallel PHEV bus also has been studied in [32].

### 2.2.2 Powertrain Components

Several different components have been considered for sizing in the literature. Many studies have focused on individual component sizing, such as the battery [9,13,14,17,18,22,33]

or electric motor [10]; however, powertrain component sizing, as an entire sub-system, has received more attention. The target in these cases is to size the key powertrain components, such as the engine, electric motor, and battery in a way that, together, they meet the requirements of the vehicle under different driving conditions, including braking, accelerating, or cruising.

Several studies on battery sizing [9, 13, 14, 17, 18, 22, 33] have been undertaken; among them, Tara et al. [22] showed that NiMH battery technology is a viable alternative to Lithium-ion (Li-ion) batteries due to its lower cost and its acceptable volume and weight. However, Li-ion battery technologies are undergoing further development to reduce cost, possibly making them the best option for future HEVs/PHEVs.

### 2.2.3 Optimization Algorithms

There are a number of methodologies used to address hybrid vehicle component sizing. Due to the various design variables and their effects on performance objectives, HEV component sizing optimization can be dealt with as a constrained non-linear optimization problem [32]. The optimization algorithm is one of the main issues in optimal sizing. Dynamic Programming [34], Particle Swarm Optimization [31], Genetic Algorithm [29, 30, 35] and, in general, evolutionary algorithms are among the most commonly applied optimization methods in recent HEV component sizing studies. Evolutionary algorithms mimic natural evolutionary principles to constitute search and optimization. In general, evolutionary methods are employed to search the design space defined by the objective and constraint functions and identify a point or points that maximize or minimize the

design criteria. There are several challenges in applying these methods to design problems. For instance, gradient-based optimization algorithms, such as the well-known Sequential Quadratic Programming (SQP algorithm), can run into trouble when inaccurate gradient information is used to determine the search directions and convergence. Derivative-free optimization techniques can be used to address these issues; however, they require many more iterations and/or function evaluations, which may make them impractical. Another way to address these problems is to integrate a local search algorithm with a global one, such as a Genetic Algorithm (GA). This could help to overcome deficiencies in both methods, like the probabilistic characteristics of GA or trapping in local minima in SQP. Basically, GA limits the search space and is suitable for non-linear objective functions. Liu et al. [35] developed a new algorithm, combining the global search ability of GA and fast convergence ability of SQP that resulted in a good convergence speed.

Fellini et al. [36] classified the algorithms currently used in the hybrid powertrain system design environment into gradient-based, derivative-free and metamodels, and used two derivative-free optimization algorithms, namely DIRECT (Divided RECTangles) and Complex, to solve the HEV optimization problem. Both algorithms were able to converge to approximately the same solution; however, DIRECT, which is a sampling algorithm, proved to be the most efficient for some sizing problems [35]. This algorithm has (Figure 2.1) fast convergence because it divides the domain into rectangles and finds the minimum by evaluating the objective at the midpoints at each iteration [37].

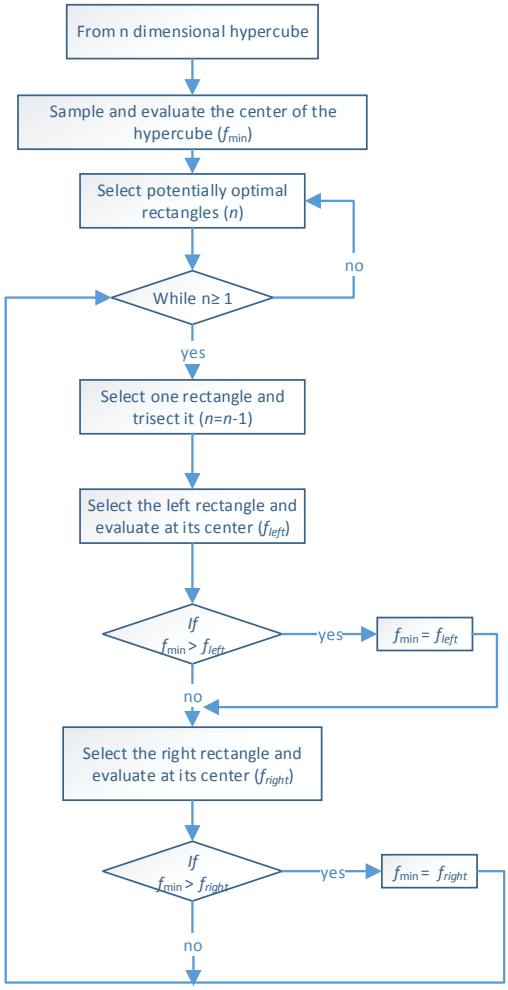


Figure 2.1: Flow chart of DIRECT algorithm

In terms of optimization objectives, most studies have targeted a single and primary optimization objective, typically fuel consumption reduction [35, 36]. However some studies consider more than one objective for optimization; for example, many simultaneously

target increased vehicle fuel economy as well as reduced emissions [28–31, 34, 36, 38], such as Hydrocarbons (HC), Carbon Monoxide (CO) and Nitrous Oxide (NOx), or improving vehicle performance [27, 28, 31, 34, 38, 39]. These objectives may conflict with each other in some situations; to achieve lower fuel consumption we might have to downsize the engine, which will consequently affect vehicle performance. In other words, optimal solutions are often not unique. In a multi-objective optimization problem without any further information about the requirements and conditions, it would be difficult to choose one solution over another. One solution for multi-objective optimization problems is to convert them into single objective problems by giving weight to each objective based on its importance [38].

Chirag et al. [32] proposed a multi-objective genetic algorithm (MOGA) method for the drivetrain sizing of a parallel PHEV transit bus, taking into consideration fuel economy and emissions as design objectives. PSAT was used to evaluate the modeled PHEV.

Shahi et al. [40] proposed a method using a Pareto Set Pursuing (PSP) multi-objective optimization algorithm to find the optimal combination of battery, engine and motor to turn a 2004 Prius (included in PSAT) into a PHEV model. An optimal combination was derived from a given set of battery, engine and motor types considering some constraints and taking reduced fuel economy, emissions and cost as objectives. The optimization problem was resolved into two sub-problems: i) defining the battery size with respect to AER (All Electric Range); and ii) finding appropriate engine and motor sizes to satisfy the required acceleration performance. This strategy significantly reduced the optimization time. Matlab functions of FZERO and FMINSEARCH were used to size the battery, and engine and motor sizing, respectively.

A set of constraints should be applied on the optimization problem to ensure that meeting the objectives does not compromise desired vehicle performance. Gradeability, acceleration time (0 to 60 mph), and AER [32,40] have been considered the most important constraints thus far in the literature.

Researchers have evaluated the objective function by running simulation and optimization models on different driving cycles, including actual driving profiles or standard cycles. Only a few studies have evaluated HEVs on a real-world driving pattern. Tara et al. [22] used recorded data from a number of vehicles to produce a real-world daily driving profile representing average behaviour. Road specifications (such as specific speed limits, traffic signs, etc.) for different segments of a specific area are required to generate a drive cycle. However, standard test procedure cycles have been used widely in the literature. Rahman et al. [41] utilized a highway drive cycle (HWFET) for simulation and evaluated their sized PHEV model against an HEV model in ADVISOR.

Although this review has covered component sizing optimization only, it should be clear that the optimization of control of propulsion systems as post-sizing design constraints will lead to greater overall efficiencies for HEV/PHEV technologies.

## 2.3 Summary

Briefly, it can be concluded that limited work has been done on the component sizing of a PHEV with a power-split configuration. Due to the high potential for this type of vehicle to increase fuel economy and reduce related environmental impacts, we have worked to

address the component sizing of a power-split PHEV. We took a relatively new approach in using Autonomie as a simulation tool to develop a plug-in Prius model.

# Chapter 3

# Plug-in Prius Powertrain Modeling and Performance Evaluation

Modeling and simulation play important roles in the success of HEV/PHEV design and development as they reduce both time and cost of production. The ability to use models in virtual environments eliminates excessive work, eases the application of design modifications, and consequently postpones prototyping to later in the design cycle, thus accelerating the design cycle.

## 3.1 Modeling in Autonomie

Autonomie, a vehicle simulator, which is a new version of the Powertrain System Analysis Toolkit (PSAT), was used to build a sizing optimization model. Autonomie contains a

library of vehicle models and components that have been collected and tested at Argonne National Laboratory (ANL) [42]. On the basis of a default PHEV model provided in Autonomie, we created a platform for a plug-in Prius (Prius model 2012).

Second and third generation Toyota Prius models, Toyota Hybrid System (THS) I/II, already exist in the Autonomie library. The plug-in model differs from these models mainly in the size and type of battery; plug-in hybrids require a larger battery capacity. That being said, the engine and electric motor are also different sizes, requiring scaling processes to be introduced. Ultimately, by using the default PHEV model and considering its differences with the 2004 Prius (THSII or Prius MY04), along with the parameters and data available for Prius 2012, we developed a model in Autonomie that can be used for optimization as well as other applications, such as control validation.

To build the model, the vehicle characteristics, powertrain configuration, and specific components must be defined. We chose a two-wheel drive PHEV with a power-split configuration as a platform. All specifications, except the vehicle mass, were set according to values available in the Autonomie Prius model. For example, the frontal area and drag coefficient were set to 2.25 $m^2$ and 0.26 respectively. All the specification except the mass of vehicle are set according to their values in the Prius model already exists in Autonomie. The vehicle mass was set to 1,525 $kg$ [43]. The chassis mass is 824 $kg$.

Table 3.1: Prius characteristics

| vehicle characteristic | Value |
|---|---|
| $\rho$ | 1.23 $kg/m^3$ |
| $C_D$ | 0.26 |
| $A$ | 2.25 $m^2$ |
| $m$ | 1525 $kg$ |

The top level Simulink model shown in Figure 3.1 includes the driver, vehicle powertrain architecture (VPA), and vehicle powertrain controller (VPC) (with the default controller).

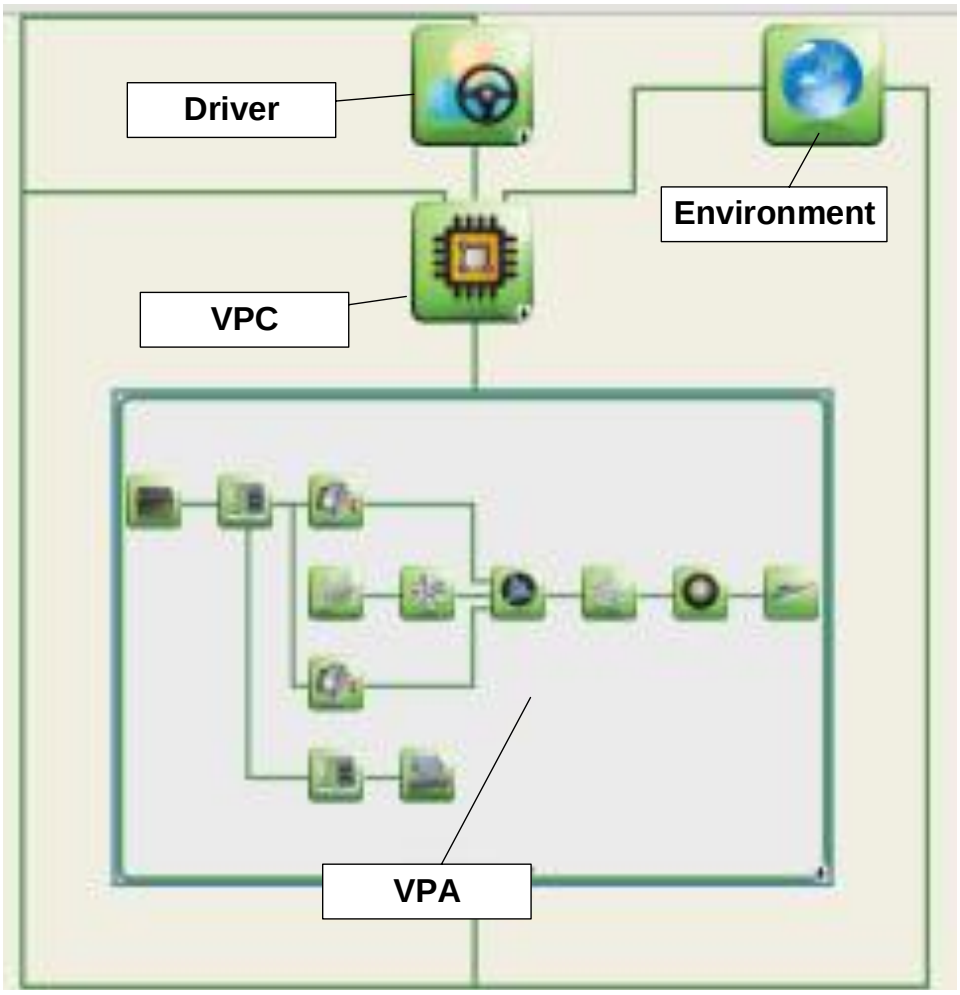


Figure 3.1: Vehicle model in Autonomie environment

In order to give an idea of how the whole system works, a detailed description of each model is provided below.

## 3.2 Powertrain

The powertrain configuration in Autonomie is shown in Figure 3.2. The main components of the powertrain are: an ICE (Eng in the figure), two electric motors (more specifically, a traction motor ($m_1$) and a generator ($m_2$)), a planetary gear ($Gb$), a battery pack, a differential ($Fd$), a chassis, wheels ($Whl$), and power convertors ($PC_1$ and $PC_2$). The model specification of each powertrain component is given below.

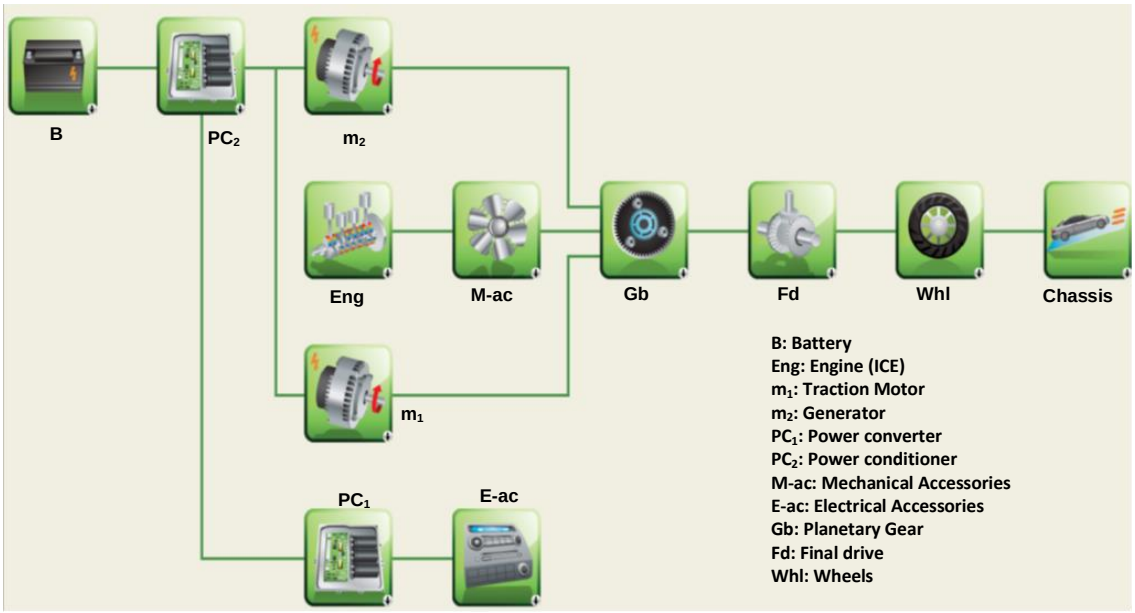


Figure 3.2: VPA power-split powertrain configuration

### 3.2.1 Engine

The engine, which is the main power supply in conventional vehicles, was modeled using look-up tables based on the engine torque and speed. The Prius 2012 has a 1.8L spark

ignition engine with maximum power of 73 kW. However, because the Prius MY04 engine (maximum power 57kW) was the default engine platform in our model, this engine had to be scaled up to be compatible with the Prius 2012. This was done using a linear engine scaling algorithm that linearly scales the fuel map. The data for this engine were measured and compiled at ANL and are available beside the scaling files in Autonomie; therefore, the fuel consumption and emissions can be calculated in this map-based engine model. Engine efficiency maps for the Prius MY04 and 2012 (after scaling) are given in Figure 3.3.

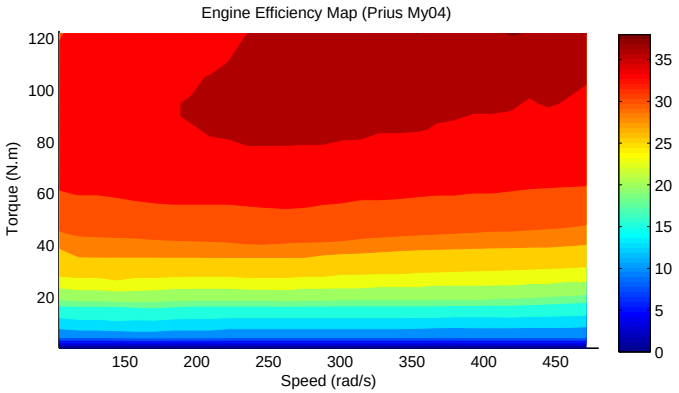


(a) Before scaling

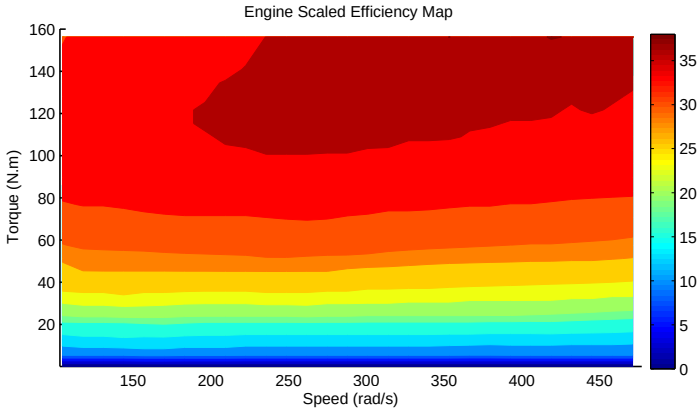


(b) After scaling

Figure 3.3: Engine efficiency maps before and after scaling

### 3.2.2 Electric Motors

As mentioned earlier, the power-split configuration utilizes two electric motors. The models for these two permanent magnet electric motors are to some extent similar to each other, and the same as the engine using look-up tables in their plants. The inputs to the maps are voltage and speed of the motors, which give current as output. Data, such as inertia

and motor efficiency maps, were provided by Oak Ridge National Laboratory (ORNL) and have been included in Autonomie. We used the models and maps provided in Prius MY04 for our model; however, we had to scale them, using the same process as was used to scale the engine model, to ensure compatibility with the Prius 2012. According to the literature [22, 24, 44, 45], the peak power of the traction motor would rise from 50 kW in the Prius MY04 to 60 kW in the Prius 2012. The other motor, called the generator ($m_2$) in this case, has a peak power of 30 kW.

### 3.2.3 Battery

As described above, the battery is the main difference between PHEVs and HEVs. We chose the Lithium-ion battery, which is the prominent battery type used in power-split HEVs, for our vehicle model. The battery pack, according to Prius 2012, consists of 4 modules of 14 elements connected in series with 21Ah capacity. This battery, developed by Saft, uses 3.7 volts/cell. The battery capacity of the default PHEV in Autonomie is different from what is required for the Prius 2012; therefore we had to correct the battery specifications and parameters in the default PHEV battery to better align them with those of the Prius 2012. In other words, a manual scaling process was applied to the battery, and increasing the cell number and battery capacity in this way allowed us to linearly increase the voltage and power of the battery pack. The battery plant receives current as input and calculates the state of charge (SOC) required by the controller. This model includes a constraint block that uses PI controllers. It also contains charging and discharging maps which take current as input and give open circuit voltage and resistance values based on

the SOC of battery. It should be mentioned that in this battery the initial SOC and the minimum SOC were set to 0.9 and 0.2 respectively [46].

### 3.2.4 Power Accessories

The electrical and mechanical accessories simulate the vehicle's power loss due to different loads from the air conditioner, lights, pump and so on. A constant power loss of 300W was considered [47].

### 3.2.5 Power Electronics

As can be seen from the configuration(Figure 3.2), there are two power converters, the $12v$ DC-DC converter used for the electrical accessories ($PC_1$) and one used for electric motors($PC_2$). These converters were modeled with the constant efficiency of 0.95 [48, 49].

### 3.2.6 Transmission

According to information provided by the manufacturer, the Prius 2012 has two sets of planetary gears. One splits the power flow from the engine and the other works as a reduction gear for the motor [44]. The Electric Variable Transmission (EVT) efficiency is calculated in Autonomie whereas the maximum efficiency is 0.98. Numbers of sun ($N_s$)and ring teeth($N_r$) are 30 and 78 respectively [50, 51]. The final drive ratio was set to 4.1130 with a constant efficiency of 0.97.

### 3.2.7 Vehicle Longitudinal Dynamics

#### Wheels

For the wheels, a 15 inch rim diameter was selected with the tire identification P195/65 R15 [52,53]. The rolling resistance force $F_R(N)$ can be calculated in the wheel model from the following equation:

$$F_R = (c_{rr} + c_{rr}^{'}V)mg \tag{3.1}$$

where $c_{rr}$ and $c_{rr}^{'}$ are the first and second rolling coefficients. The first represents a typical friction coefficient due to a normal force and is set to 0.008, while the second is set to 0.00012 in $s/m$ [1]. In addition, $V$ is the speed of the vehicle in $m/s$, $m$ is the mass of the vehicle in $kg$, and $g$ is gravity, 9.81 $m/s^2$, in the above equation.

#### Chassis

The chassis model contains the dynamics of the vehicle. The real velocity of the vehicle is calculated based on the basic dynamic equations. Prius model MY04, available in the Autonomie library, utilizes a coefficient-based model for chassis, wheel, and driver models. This means that instead of using the vehicle dynamic equations, coefficient-based models use some coefficients obtained from the tests carried out in ANL; however, for the Prius 2012 we used an equation-based vehicle dynamic model considering forces of drag, rolling resistance, and forces due to the road grade. As mentioned previously, the chassis model should be compatible with the driver and wheel models. Thus, in this case we had to choose equation-based models for the wheels and driver as well. All the vehicle specification

parameters, such as mass, frontal area, gear ratio, and, in general, the whole data for the Prius 2012 were derived from the literature [22, 24, 44, 45, 50], Toyota website [53] and experimental test results provided by ANL.

### 3.2.8 Interconnection Between Powertrain Components

The following block diagram (Figure 3.4) shows the input and output signals for each component in the powertrain and the interconnection between the component models.

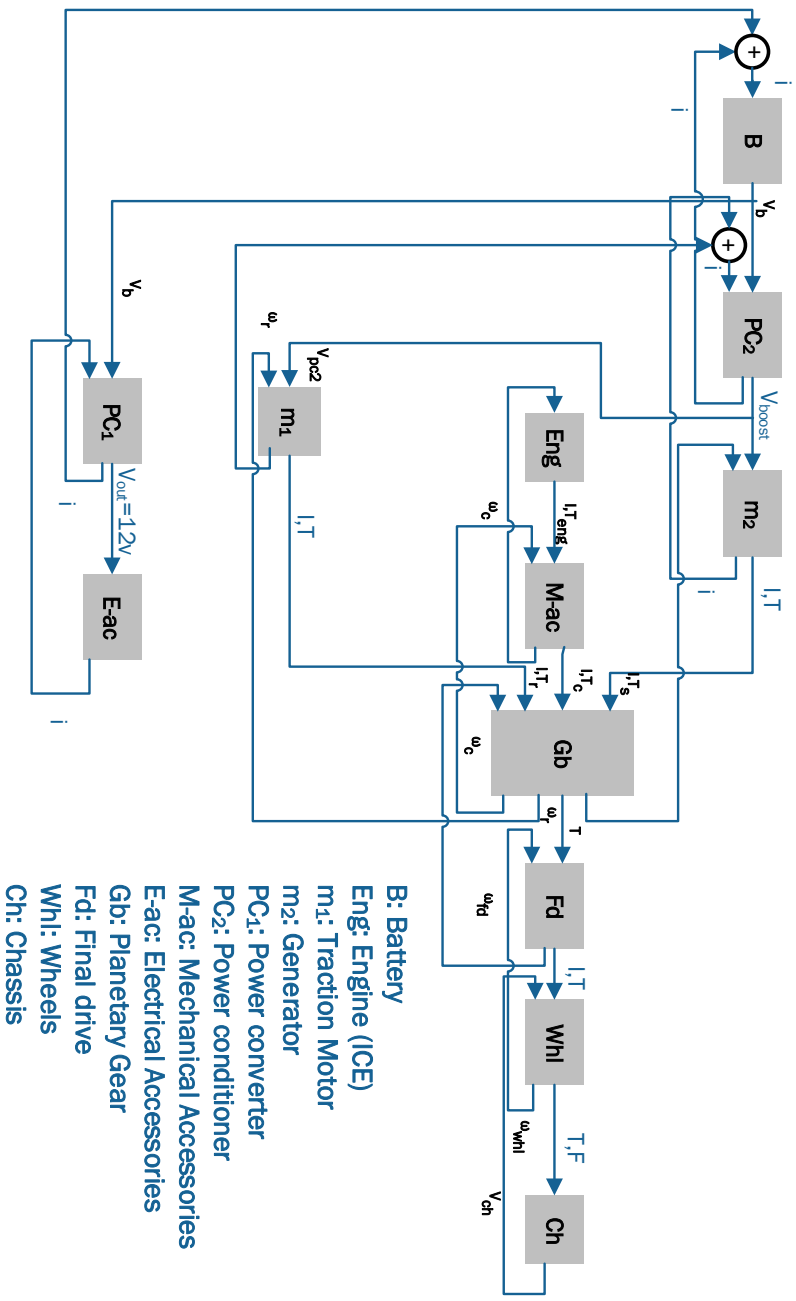


Figure 3.4: Interconnection of powertrain components

As a brief explanation, torque flows out of the engine into the mechanical accessories, the mechanical accessories apply their losses and torque is given out to the planetary gear. The engine is connected to the carrier, so the speed of the carrier is fed back to the mechanical accessories and is basically fed back thorough to the engine.

As another example, voltage is released from the battery and currents are fed back into it from each of the systems, such as the power conditioner ($PC_2$) and also 12V DC to DC converter($PC_1$) (for the electrical accessories). Electrical systems, such as the motors, are connected to the power conditioner so that voltage flows out of the power conditioner to each of the motors and a current is fed back into the power conditioner from each motor. There is a plant and a controller inside each component model (systems). All of the information from local info buses are aggregated together and then sent out and passed upwards from subsystems to the next parent systems. As a result, signals from all systems in the VPA enter into the VPC and other main blocks.

## 3.3 Driver

The driver model determines the differences between the real vehicle velocity and the velocity of the cycle according to which the vehicle should be propelled and based on which, vehicle torque loss is calculated and torque demand is determined.

It should be noted that the driver model must be compatible with the chassis and wheel models as they all use vehicle dynamics equations. Therefore, we had to choose equation-based models for the wheel, chassis, and driver models. This means these systems use

equation-based models within them instead of models based on some specific coefficient.

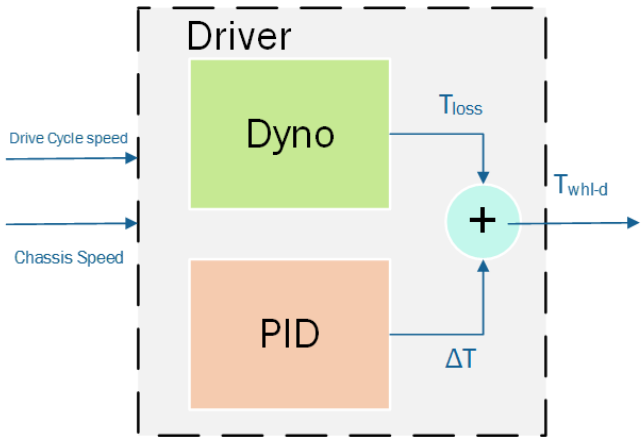


Figure 3.5: Driver model

The driver model calculates the torque demand of the vehicle based on the vehicle torque losses due to rolling resistance, drag and gravity forces which can be calculated as:

$$F = mg\sin\alpha + \frac{1}{2}C_D V^2 + C_r mg\cos\alpha + ma \tag{3.2}$$

where,$\alpha$ is the road grade, $C_r$ and $C_D$ are the rolling resistance and drag coefficients respectively. $C_r$ is obtained from the parentheses term $(c_{rr} + c_{rr}^{'}V)$ in equation 3.1. $a$ is the vehicle acceleration in $m/s^2$. Thus the vehicle torque losses would be:

$$T_{loss} = R \times F = R(mg\sin\alpha + \frac{1}{2}C_D V^2 + (c_{rr} + c_{rr}^{'}V)mg\cos\alpha + ma) \tag{3.3}$$

where $R$ is the wheel radius in $m$; $c_{rr}$ and $c_{rr}^{'}$ (in $s/m$) are the rolling resistance coefficients, the whole term $c_{rr} + c_{rr}^{'}V$ represents the total rolling coefficient calculated based on the

vehicle speed. The values for these parameters were given in Table 3.1.

The driver model (Figure 3.5) also contains a PID controller, which takes the speed error into consideration.

## 3.4 Vehicle Propulsion Controller

The top level vehicle control strategy is considered in the VPC. Based on the SOC behaviour depicted in Figure 3.6, the control strategy can be separated into two modes:

- Charge Depleting (CD): the vehicle is propelled primarily using energy from the battery, resulting in a net decrease in battery *SOC*.
- Charge-Sustaining (CS): the vehicle is propelled primarily using energy from the engine, maintaining battery *SOC* within a range (very small changes).

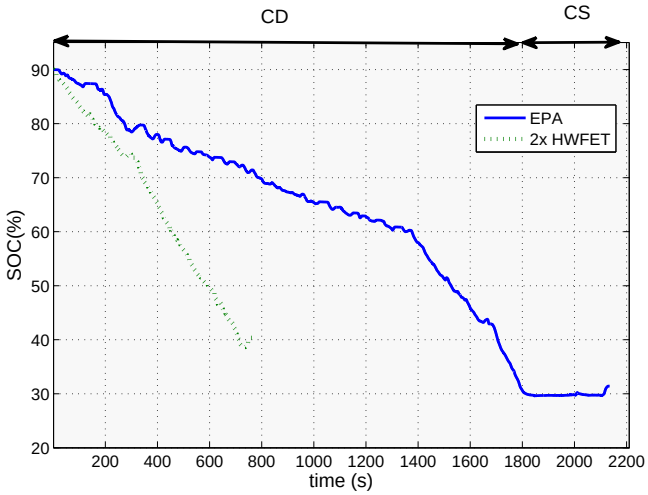


Figure 3.6: Battery State Of Charge for different drive cycles

Figure 3.6 shows the SOC behaviour for two different drive cycles of EPA and HWFET (will be explained in more detail in the next chapters). It can be observed that, in response to the HWFET cycle, the SOC did not reach the CS mode but both CS and CD mode are clearly presented in the EPA cycle.

The control strategy for power-split configurations has two subsystems: there are the propelling and brake blocks and a block to merge these together based on the vehicle mode. Figure 3.7 gives a high level depiction of the control strategy. From the figure it can be seen that the vehicle controller receives the torque demand calculated in the driver block and based on the vehicle speed it determines the vehicle mode, whether braking or propelling. The engine on/off command and its torque demand are specified afterwards. Based on this information and pre-determined values for maximum allowable motor and generator power in both regenerative and propelling modes, the controller defines the torque demand of generator ($m_2$) and traction motor ($m_1$).

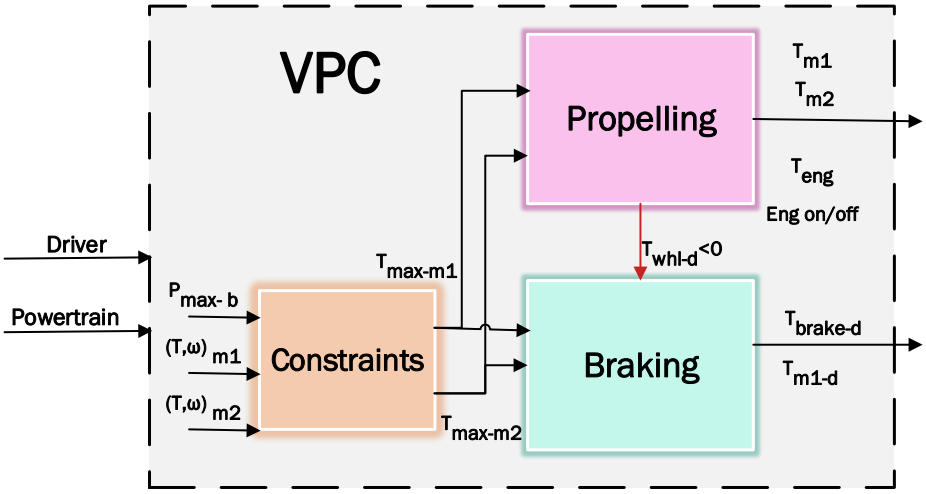


Figure 3.7: Controller model(high level)

As stated above, torque demand for the main powertrain components (engine, motor and generator) can be defined based on constraints calculated beforehand in the constraints block. The controller block diagram shows that the maximum torque at the generator and motor in different modes (whether producing electricity or consuming it) can be specified from the speed and torque of the motor and generator, the maximum power of the battery $P_{max-b}$ and using the following equation (with regard to Figure 3.2) as:

$$P_{max-m_1} = \eta_{pc_2} P_{max-b} - \frac{P_{e-ac}}{\eta_{pc}} - P_{m_2} \tag{3.4a}$$

$$P_{max-m_2} = \eta_{pc_2} P_{max-b} - \frac{P_{e-ac}}{\eta_{pc}} - P_{m_1} \tag{3.4b}$$

where $\eta_{pc}$ and $\eta_{pc_2}$ are the efficiencies of the power convertors $PC_1$ and $PC_2$ for the electric devices and battery, $P_{e-ac}$ is the power of electric accessories, and $P_{m_1}$ and $P_{m_2}$ are

the power of the electric motor and generator respectively. $P_{m_1}$ and $P_{m_2}$ can be determined from look-up tables containing relevant speed and torque values. Finally, from the calculated maximum power, the maximum allowable motor torque (or generator) can be obtained in reverse, from maps based on the power and speed of the motor (or generator). It should be noted that this torque has to be lower than the maximum torque determined in the powertrain level from the maps of the motor (or generator). Thus, this torque value indicates the maximum torque that the motor and battery can handle.

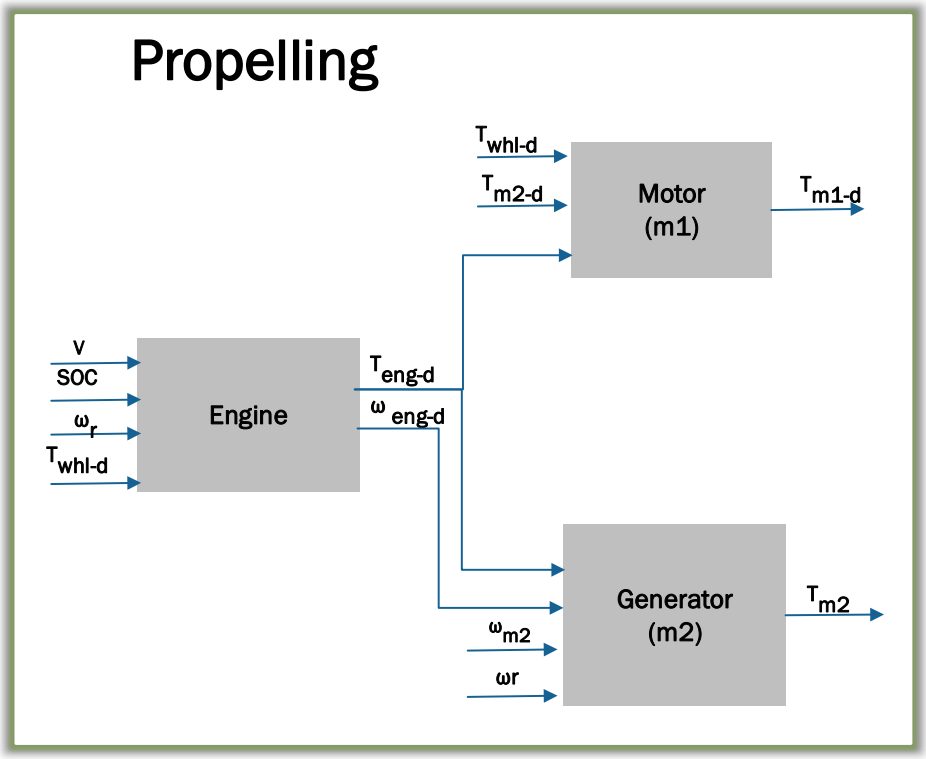


Figure 3.8: Inside VPC- propelling block

For braking and regenerative modes, equation 3.4 would take the form:

$$\left.\begin{aligned} P_{max-m_1} &= \frac{P_{max-b}}{\eta_{pc_2}} - \frac{P_{e-ac}}{\eta_{pc}} - P_{m_2} \\ P_{max-m_2} &= \frac{P_{max-b}}{\eta_{pc_2}} - \frac{P_{e-ac}}{\eta_{pc}} - P_{m_1} \end{aligned}\right\} \quad \text{Regenerative mode} \tag{3.5}$$

The torque obtained here is the same as in the previous case; it represents the maximum torque the electric system can handle.

The engine ON/OFF logic is the main and critical part of the control strategy that determines when the engine will turn on in certain scenarios (Figure 3.9):

- The requested power is above a threshold
- The battery $SOC$ is lower than a threshold
- The electric motor cannot provide the requested wheel torque

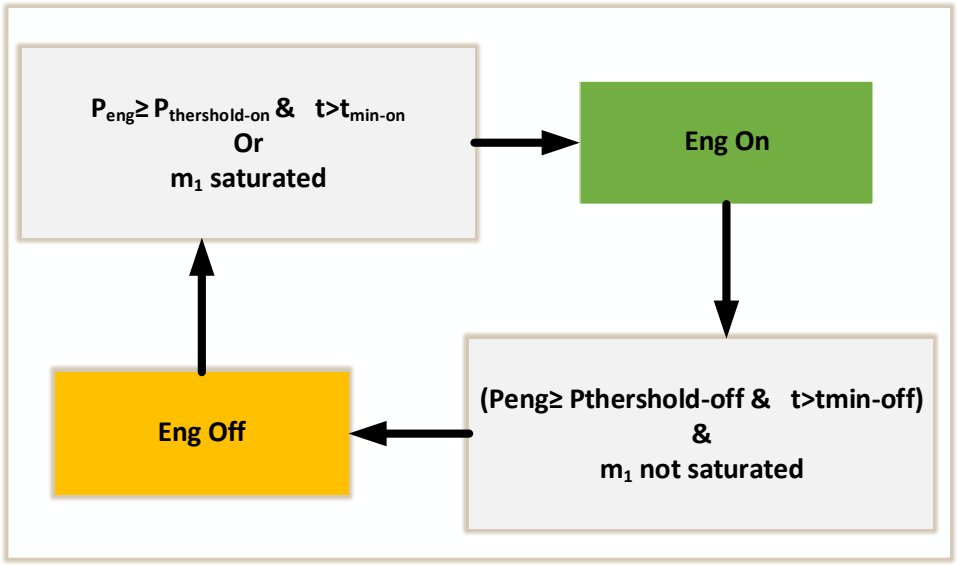


Figure 3.9: Engine ON/OFF logic

In order to determine the engine ON/OFF logic, the power term $P_{eng}$ can be defined from the following form:

$$P_{eng} = P_{chassis} + P_{b-d} \tag{3.6}$$

where $P_{chassis}$ is the requested power at the wheel and $P_{b-d}$ is the additional power to maintain the $SOC$ of the battery during CS operation. In other words, the $P_{b-d}$ function regulates the $SOC$ so that it can be positive or negative depending on the value of the current $SOC$ compared to the target. The target $SOC$ differs from the minimum $SOC$ (0.2) and represents the start of the charge sustaining mode. This parameter is set to 0.3 in the model [46]. $P_{chasis}$ is calculated from the desired speed and torque demand. Basically,

$P_{b-d}$ is calculated from the following equation:

$$P_{b-d} = k_p(SOC_{target} - SOC) + \frac{k_i}{s}(SOC_{target} - SOC) + P_b \tag{3.7}$$

where, $k_p$ and $k_i$ are the proportional and integral gain, respectively, and $P_b$ is the power derived from the maps based on the $SOC$. In our model, $k_p$ and $k_i$ values were set to zero, therefore only battery power of $P_b$ would determine the final value for $P_{b-d}$ at each $SOC$. Figure 3.10 shows $P_b$ versus $SOC$ plot for the battery model.

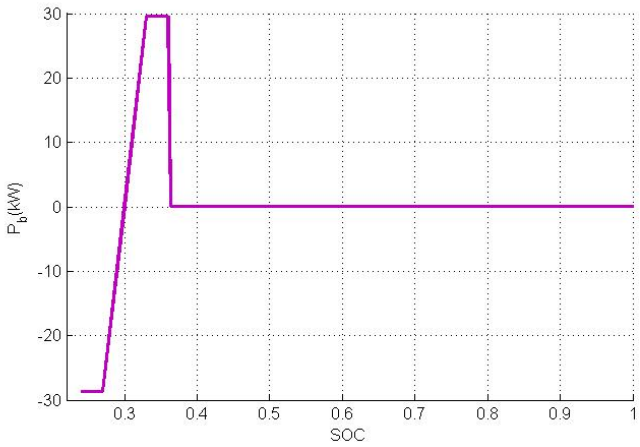


Figure 3.10: $P_b$ versus $SOC$

Once the engine power ($P_{eng}$) is known, the controller can determine the engine status using engine on/off maps of power based on the $SOC$; i.e., if $P_{eng}$ is above the power threshold for a certain $SOC$, the engine would turn on and vice versa, there is a similar map for engine off thresholds. Engine speed can be determined from the map of engine power to speed. The controller compares this speed with the one obtained from the planetary gear by having the ring speed ($\omega_r$),$N_s$ and $N_r$ (number of sun and ring teeth, respectively),

and selecting the minimum speed as the demand engine speed $\omega_{eng-d}$.

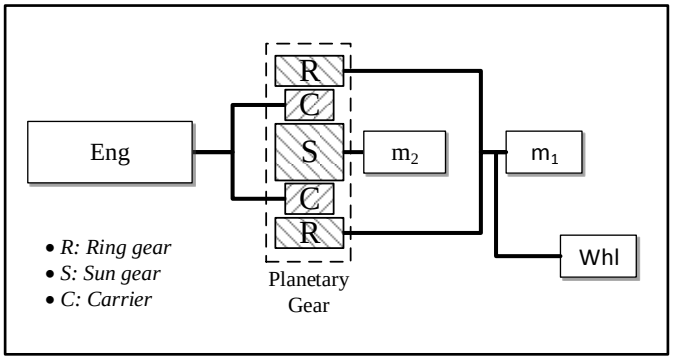


Figure 3.11: Planetary gear

Once the engine speed and power are known, the engine torque can be calculated from:

$$T_{eng} = \frac{P_{eng}}{\omega_{eng-d}} \tag{3.8}$$

This torque should be less than the maximum engine torque ($T_{eng-max}$) and the maximum allowable torque at carrier ($T_{c-max}$), otherwise the controller will replace this torque with the minimum one. $T_{eng-max}$ can be obtained from the engine map based on engine speed and $T_c$ can be derived from:

$$T_{c-max} = (T_{m_{2-max}} \frac{N_s + N_r}{N_s}) \tag{3.9}$$

Once the engine torque and speed (as well as the desired wheel torque and speed) were known, the electric machines torque could also be calculated considering the constraints and governing relations between the engine and electric motors ($m_1$ and $m_2$) in the plan-

etary gears. The resulting torque value would be delivered from the controller to relevant components in the powertrain level.

## 3.5 Overview of the Model

VPA, VPC, driver and environment blocks are interconnected via buses that contain information about the vehicle. The main info bus leaves the VPA and collects all the signals from the vehicle's powertrain systems (VPA). According to Figure 3.12, this main VPA info bus enters the VPC, driver and environment blocks. The environment block also sends its bus with all of the signals that enter into VPC. So, the main VPA info bus and environment bus come together, along with input from the driver, and they enter into the VPC where the control strategy can make used of them. Afterwards, signals from all of the VPC subsystems enter the VPA as well.

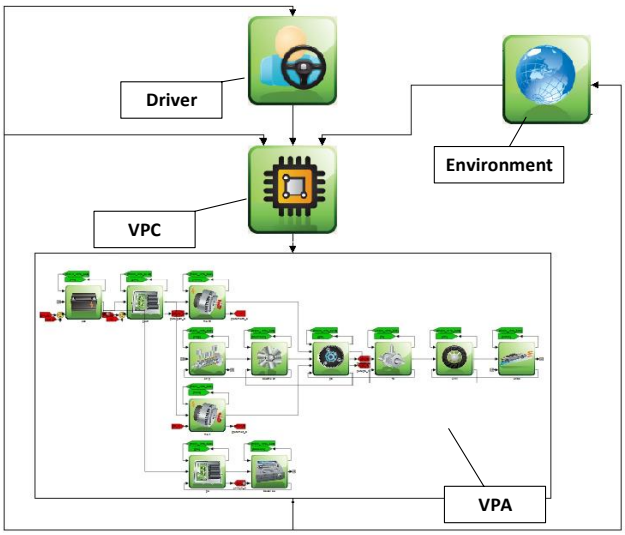


Figure 3.12: Interconnection of blocks

According to Figure 3.13, and based on the integrated nature of the subsystems (driver,VPA and VPC), torque demands are determined in the controller. Based on these torque demands, the motor and generator can feed back the obtained current to the battery. The battery will determine its $SOC$ and send it to the controller. The engine can specify the vehicle's fuel consumption based on the engine torque demand. The planetary gear can verify the speed of sun($\omega_s$), carrier($\omega_c$) and ring ($\omega_r$) gear wheels based on the specified torque demand in the gearbox. Vehicle torque and traction force would be determined in the wheel block and finally the chassis will determine the vehicle speed based on the received information.

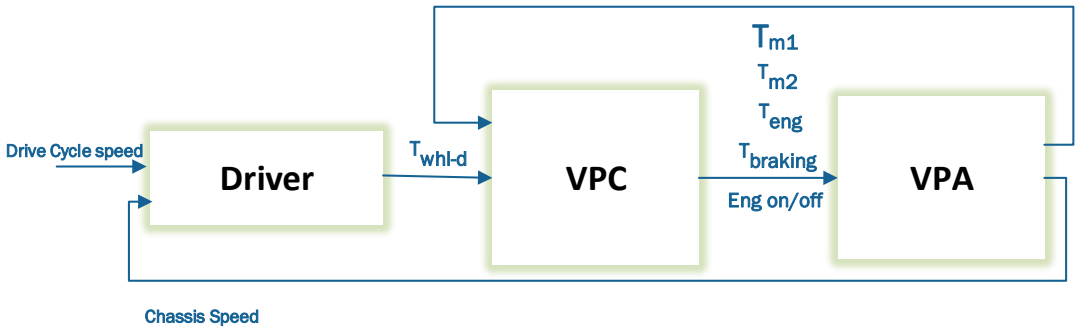


Figure 3.13: Vehicle block

In summary, all of the information from local info buses is aggregated together and then sent upwards through subsystems to parent systems and then to the next level of parent systems. This flow of information continues until it reaches the VPA level, where it is then fed back out through a powertrain bus towards the VPC, driver and environment blocks. This iterative process continues until the end of the drive cycle.

## 3.6 Evaluation

Many parameters and factors can affect a vehicle's fuel consumption. Sensitivity analyses can be important tools for identifying which parameters among many possible variables have the greatest effect on performance.

Thus, before running an optimization algorithm on the PHEV model, a sensitivity analysis was undertaken to find a trend that correlates key powertrain component sizing with fuel consumption. The advantages of this analysis are twofold: it can provide an idea

of what to expect from the optimization results beforehand and it can help validate the objective function and optimized results.

For this purpose, simulations were run for different sizes of each component, while the sizes of other components were held constant; this allowed us to directly monitor the effects of specific component sizing on fuel consumption. Here, sizing of the key powertrain components, electric motor, engine and battery, is the main goal. Therefore, the size of each of these components was varied by 10% and 20% from their initial values while the rest of the powertrain components were held constant.

According to Table 3.2, component simulations were run on EPA drive cycle (described in Chapter 4) using different engine power ($P_e$) values, while the electric motor power ($P_m$) was kept at its initial value in the model ($60kW$). The engine needed to be scaled at each level. Figure 3.14 shows the impact of engine power on fuel consumption. As was expected,

Table 3.2: Engine power values

| $P_m$ | 60 $kW$ | | | | |
|---|---|---|---|---|---|
| $P_e$ | 57 | 65 | 73 | 80 | 87 |

fuel consumption increased with increases in engine power. Therefore, it is expected that the optimization results will show that the minimum possible engine size can meet the desired performance.

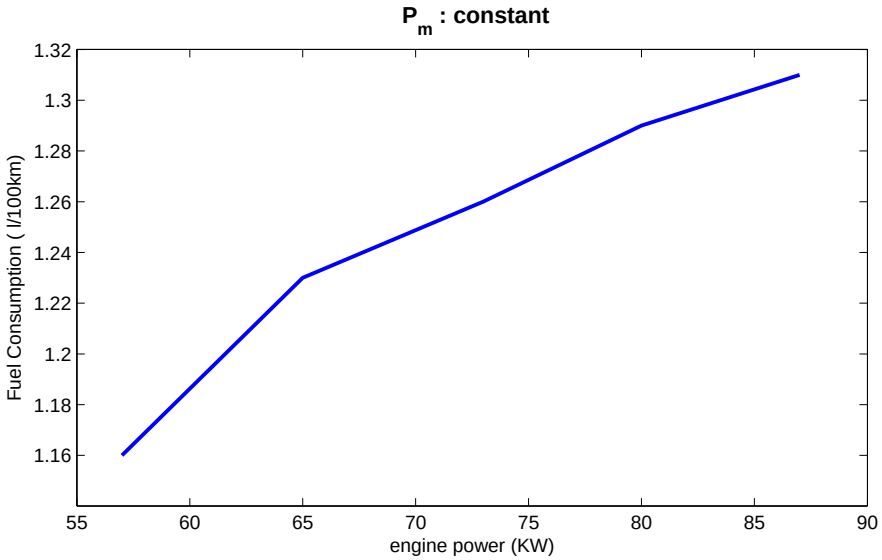


Figure 3.14: Fuel consumption versus engine power

The same process was used to analyze different values of the electric motor power (Table 3.3) on fuel consumption. This time, engine power was kept at its initial value ($73kW$) and the motor was scaled at each level.

Table 3.3: Electric motor power values

| $P_e$ | $73\ kW$ | | | | |
|---|---|---|---|---|---|
| $P_m$ | 20 | 25 | 30 | 50 | 70 |

For the most part, the fuel consumption curve built based on varying electric motor power (Figure 3.15) follows a pattern similar to that seen in response to large engine sizes (high power). However, at small electric motor power values, fuel consumption behavior deviates considerably from the expected trend. This can be explained based on the power

distribution between the engine and the electric motor, where the engine is required to propel the vehicle because of the electric motor capacity is too small. Therefore, the motor could not provide the required power even if the engine efficiency was low, and as a result more fuel was consumed.

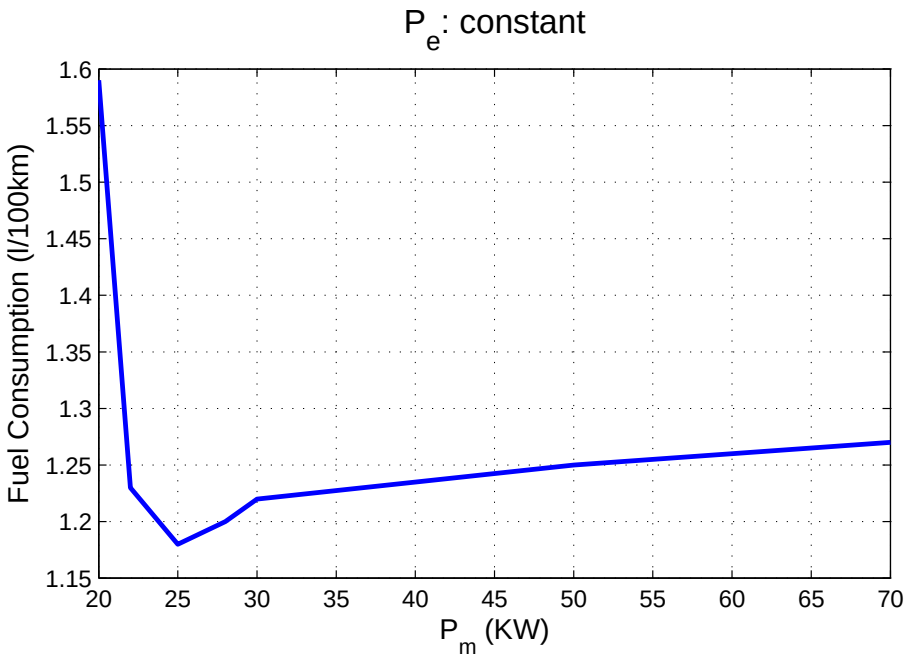


Figure 3.15: Fuel consumption versus electric motor power

In Figure 3.15, there is an optimum point that identifies the electric motor power size required to achieve minimum fuel consumption. For power values larger than this optimum, fuel consumption increases again. This fact can be explained using the electric motor efficiency map (Figure 3.16). Figure 3.17 shows the motor efficiency in terms of power for different angular velocities. Optimum points with higher efficiencies are clear in this map. Therefore, for larger powers the optimum efficiencies do not match the working

points of the motor in the considered drive cycle. This means they had lower efficiencies than the optimum, resulting in increased fuel consumption.

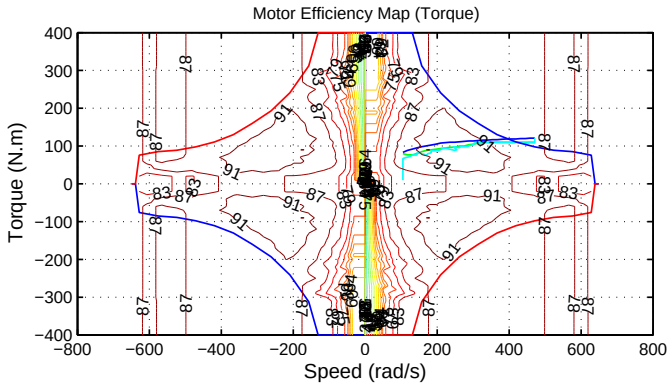


Figure 3.16: Electric motor efficiency map

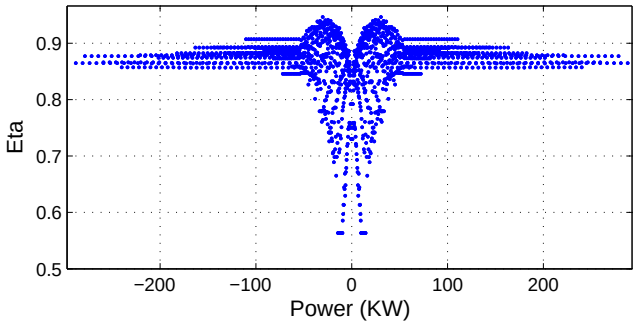


Figure 3.17: Electric motor efficiencies versus power for different working points (angular velocities)

This same process was used to analyze battery capacity sizing on fuel consumption as well. Larger battery capacities led to lower fuel consumption (Figure 3.18). This reflects the fact that, with a small battery pack, the controller mostly uses the engine to propel

the vehicle. And, in contrast, the smallest battery pack sizes led to high fuel consumption rates - and these rates kept increasing until the engine's power could not match the power demand, forcing the battery to provide the remaining required power.

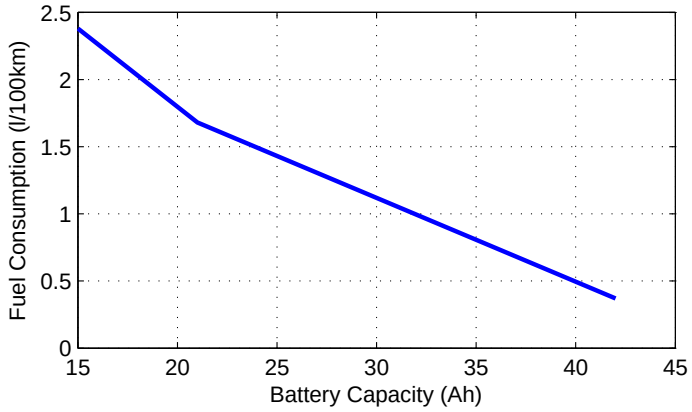


Figure 3.18: Fuel consumption versus battery capacity

The vehicle's power demand can be obtained from the dynamics of the vehicle, based on drag and rolling resistance forces at specific times and speeds. Therefore, after obtaining the traction force F from equation 3.2, the power demand can be derived as:

$$P = FV \tag{3.10}$$

Based on equation 3.10, the power required to cruise the vehicle at different speeds and road grades can be calculated. For instance, from equation 3.10 it is clear that the current engine (the Prius engine with 73 $kW$ kW peak power) would be sufficiently powerful to cruise the vehicle at 40 $m/s$ and with 1% road grade. This potentially presents an opportunity to downsize the electric motor and battery by assuming a fixed size for the engine.

So far we have considered the impact of different component sizes on fuel consumption without paying attention to the possible consequences they might have on other vehicle performance parameters. It is important to achieve a significant reduction in fuel consumption; however, this should not be at the expense of desired vehicle performance. In this regard, the sensitivity analysis was followed by an acceleration test, which allowed us to observe changes in acceleration time caused by changes in electric motor size.

The desired vehicle performance was chosen according to PNGV (Partnership for the Next Generation of Vehicles) goals [1, 54, 55], namely that the vehicle can accelerate from 0 to 60 $mph$ ($96km/h$) in less than 12 seconds. Throughout this procedure, the engine and motor worked together to provide the required power. If the engine size was assumed fixed and according to its value in Prius 2012, the size of the electric motor could be determined by subtracting the engine power from the total required power. It is clear from Figure 3.19 that the engine can solely provide the required power for accelerating from 0 to 60 $mph$ in the desired time. Therefore, a smaller electric motor can be used here provided that the required performance of the vehicle is satisfied.

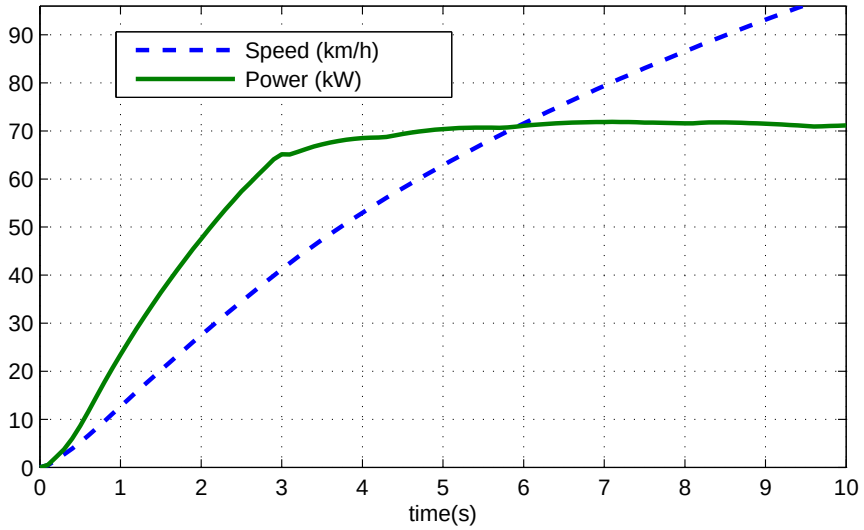


Figure 3.19: Power demand for the Prius acceleration test

As stated above, the acceleration test for different electric motor sizes was run in order to consider its effect on the 0-60 $mph$ acceleration time. Table 3.4 shows that the results aligned with our expectations; the acceleration time increased with a reduction in the electric motor size. The acceleration time for the default motor($P_m = 60kW$) in the Prius 2012 was close to the acceleration time of the real vehicle, achieving 0-60$mph$ in 9.7$s$ [52,56]. This fact can be used as a cross validation for our model with acceptable error (3%) for the acceleration time of 0-60 $mph$.

According to Table 3.4, and in order to maintain an acceptable vehicle performance using the Prius engine (peak power of 73 $kW$), an electric motor with peak power of more than 40 $kW$ would be preferred.

Table 3.4: Acceleration test results

| $P_m(kW)$ | $t(s)$ | Fuel Economy(MPG) |
|---|---|---|
| 70 | 8.7 | 20.08 |
| 60 | 9.4 | 20.05 |
| 50 | 10.9 | 19.97 |
| 40 | 12.8 | 19.75 |
| 30 | 15.6 | 19.44 |
| 20 | 20.1 | 18.96 |
| 15 | 23.6 | 22.3 |
| 10 | 35.8 | 21.85 |

Table 3.4 also includes fuel economy values. Fuel economy (fuel consumption) increased (decreased) with increased in motor power. The table also reveals the same trend for the very small motors as seen in the case for fuel consumption in the EPA cycle. In other words, fuel consumption did not follow a specific trend (increasing or decreasing) as the electric motor size increased.

Consequently, the overall vehicle performance is directly related to the performance of each powertrain component.

In addition to the model evaluation activity described above, the model was cross-validated against a PHEV model developed in MapleSim [57]. 1.7 $l/100km$ predicted fuel consumption by the MapleSim model in [57] was in response to 2 successive FTP drive cycle, where the model developed in Autonomie showed fuel consumption rates of

1.7 $l/100km$ for this cycle. There is an acceptable margin of 5% error between these two models. Therefore, with a good estimation, the Autonomie model was validated.

# Chapter 4

# Optimal Sizing of Powertrain Components

PHEV/HEV powertrain configurations are more complicated than conventional ICE powertrains, owing to the addition of electrical components such as electric motors and generators. Therefore, it stands to reason that PHEV/HEV component sizing optimization is also more difficult as many new design variables must be considered. The number of battery cells, maximum engine and motor power, as well as controller parameters are key examples of these variables.

Several optimization methods have been considered to address PHEV/HEV sizing. Each can generally be classified according to whether it is a gradient-based or derivative-free, deterministic or stochastic, and local or global optimization method. HEV/PHEV powertrain sizing involves a variety of design variables, constraints, and objectives, making

the optimization problem non-linear with numerous local minima or maxima. Therefore, methods that do not require derivative information and do not get trapped in local minima or maxima are the most appropriate to address optimization of these complicated platforms. Therefore, while gradient-based and local optimization methods demonstrate higher rates of convergence, owing to the above-mentioned challenges, derivative-free and global optimization methods have received more attention for sizing purposes in the literature [29, 32, 34, 35, 38].

Most PHEV/HEV optimization problems have two or more objectives to be simultaneously addressed, and these objectives may often conflict with each other. Classical methods for solving multi-objective optimization problems usually map multiple objectives into a single objective and solve it one would a single objective problem. An alternative solution is to integrate several different optimization algorithms together, taking advantage of the benefits from each individual algorithm while, at the same time, eliminating their drawbacks. This method also decreases computational time, saving design and production costs.

Evolutionary Algorithms (EA), such as Genetic Algorithm (GA), and similar techniques, such as Particle Swarm Optimization (PSO) and Dynamic Programming (DP), are among the many methods widely used for PHEV/HEV design optimization and component sizing to meet fuel consumption, emissions, cost and other ambitious objectives. These popular techniques provide very efficient solutions for multi-objective optimization problems. Some are reviewed in the next sections.

## 4.1 Particle Swarm Optimization

Particle Swarm Optimization (PSO) is a stochastic and population-based search algorithm developed by Kennedy and Eberthart in 1995 [58]. It is mainly inspired by social behaviour withing natural systems, where large groups of individuals interact, such as in flocks of birds, schools of fish, or swarms of bees, and even human social systems. The working principle behind the PSO algorithm is based on the simulation of a simplified social system; for instance, the behaviour of a flock of birds flying across an area seeking a location with abundant food.

A PSO model consists of particles moving in a multi-dimensional search space, interacting with their group. Each of the particles has two properties, a current position and a velocity. Each particle remembers the best position it has experienced thus far in the search space (among the swarm) and is also aware of the best-reached position of the group so far. By considering the individual experience of each particle, which is the memory of its best past position, and the experience of the most successful particle, the PSO algorithm will predict the best next position for the particles at each iteration. Therefore, at each step each particle moves with a velocity dynamically adjusted according to its own history (experience), and those of its peers, which consequently result in global behaviour. Based on this principle, the global optimum in optimization problems can be obtained.

Owing to its easy implementation and simple equations, PSO can be applied to address the optimization of hard mathematical problems.

## 4.2 Dynamic Programming

Richard Bellman developed Dynamic Programming (DP), a numerical method based on the principle of optimality, in the 1950s [59]. Similar to other optimization methods, this global optimization approach aims to minimize the cost function while satisfying relevant constraints. The term "dynamic programming" is a bit misleading as it simply refers to multi-stage decision processes. DP algorithms solve optimization problems by setting a table and filling each spot in the table based on the other values in the table.

DP is widely applicable to complex optimization problems because it reformulates the problem using a decomposition process. As a result, the n-variable problem breaks down into n simplified one-variable (sub-) problems, each of which will be solved only once and saved in a table. Afterwards, solutions for each sub-problem are combined together to yield an overall solution. This dramatically reduces both computational time and effort. In employing DP, there are some constraints on the problem that should be held, such as non-negativity of the objective function.

## 4.3 Genetic Algorithm

Genetic Algorithm(GA) [60] belongs to the set of Evolutionary Algorithms (EA), which are based on natural evolutionary principles. GA limits the design space using a natural selection scheme, which distinguishes it from traditional methods that use gradient information to find optimum values. Therefore, GA is an efficient method for problems with large design spaces. GA and PSO are very similar; the selection process in GA is

substituted for a memory (for best social and individual location) in PSO.

According to the procedural flowchart shown in Figure 4.1, this stochastic approach starts by randomly generating the initial population of solutions based on the range and constraints of the design variables. Afterwards, GA narrows the search space by selecting the best solution among the parent population using different operators, namely mutation and crossover. These operators create a new generation of "better" solutions by selecting and modifying current solutions to omit those that are bad. This natural selection procedure, where only the best solutions survive, continues until the end criterion is met.

The deficiencies of GA, due to its probabilistic characteristics and slow convergence rates, can be addressed by combining it with a local gradient-based method that can help to achieve a satisfactory convergence speed.

GA has been widely applied to HEVs/PHEVs sizing problems.


Figure 4.1: GA flowchart

## 4.4 Proposed Optimization Methodology

In our approach, GA was integrated with Autonomie as a simulation tool to create a framework that can optimize PHEV powertrain components. As previously discussed, GA

is considered an efficient method for optimal sizing of HEV and PHEV platforms.

Thus, GA combined with Autonomie, which can simulate both vehicle performance and fuel consumption, provides a strong tool for complex PHEV component sizing optimization.

As explained in Chapter 3, a power-split PHEV was modeled in Autonomie using Prius model 2012 specifications. This PHEV model was initially simulated using design values given in Table 4.1. $P_{eng}$, $P_{motor}$, and $N_b$ denote the engine power, motor power and number of battery cells, respectively.

Table 4.1: Initial design value

| Parameter | Value |
|---|---|
| $P_{eng}$ | $73kW$ |
| $P_{motor}$ | $60kW$ |
| $N_b$ | 56 |

For these initial values, the objective function, which is the fuel consumption for a specific drive cycle, was evaluated and determined. The results were then fed back into the optimization algorithm, allowing GA to identify new design values. The model was simulated with these new values and the objective value was determined. Again, the simulation results were reported back to the GA, which generates a new set of design variables. This iterative procedure (Figure 4.2) continued until the stopping criteria was reached (the maximum number of generations, typically 20).

After the design parameters were optimized, the resulting vehicle design would have a different weight from the initial weight (Prius mass). Therefore, the weights of the resulting

designs were scaled and the new vehicle mass was calculated.

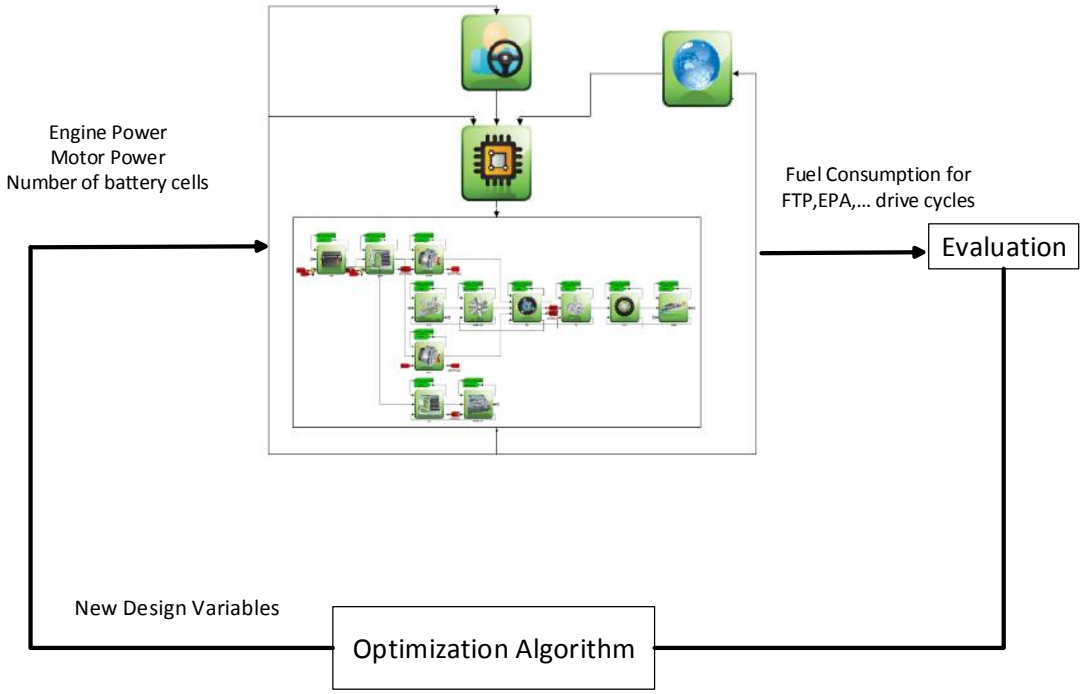


Figure 4.2: Optimization process

Figure 4.2 illustrates the whole framework of the methodology. Similar procedures have been used in the literature to address vehicle platforms [35, 61]. It should be mentioned that the design variables were restricted within their bounds. These bounds should be determined based on the vehicle performance requirements, as discussed later.

## 4.5 Drive Cycle

An appropriate driving cycle, which properly represents the vehicle behavior, should be selected. The optimization must be run over different drive cycles in order to minimize the fuel consumption across the driving profile. For example, highway driving requires more power and as a result requires larger motor and engine components, on the other hand, driving at low speeds or in urban areas, where frequent stopping, idling and braking is required, does not impose high vehicle performance demands; thus, small engine and motor components would be sufficient to meet performance expectations. In this study, we considered the effect of several different driving cycles, including urban, highway, and a combination of both cycles.

The FTP cycle (Federal Test Procedures) specifications, which characterize the urban driving experience, are given in Table 4.2. It is obvious from Figure 4.3 that during this urban cycle, which has a maximum speed of $96km/h$ and total distance of $17.77km$, the vehicle could be propelled by power derived from the motor and batteries, with very little input from the engine. Therefore, we used a multiple of this cycle in order to achieve nonzero fuel consumption.

Table 4.2: FTP characteristics

| Description | Value |
|---|---|
| $TotalTime$ | $2477s$ |
| $Distance$ | $17.77km$ |
| $AverageSpeed$ | $42.2km/h$ |
| $MaxSpeed$ | $91.2km/h$ |
| $MaxAcceleration$ | $1.47m/s^2$ |

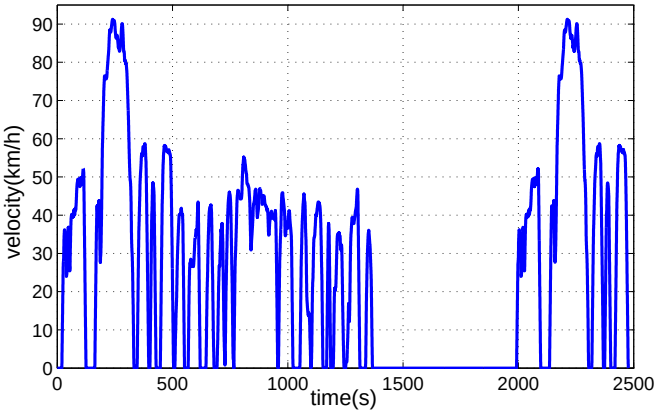


Figure 4.3: FTP drive cycle

The HWFET (HighWay Fuel Economy Test) drive cycle is shown in Figure 4.4, and the specifications are given in Table 4.3. For the same reason as in the case of the FTP cycle, we had to use a $2 \times HWFET$ for simulation and further optimization.

Table 4.3: HWFET characteristics

| Description | Value |
|---|---|
| $TotalTime$ | $764s$ |
| $Distance$ | $16.5km$ |
| $AverageSpeed$ | $78.2km/h$ |
| $MaxSpeed$ | $96.4km/h$ |
| $MaxAcceleration$ | $1.43m/s^2$ |

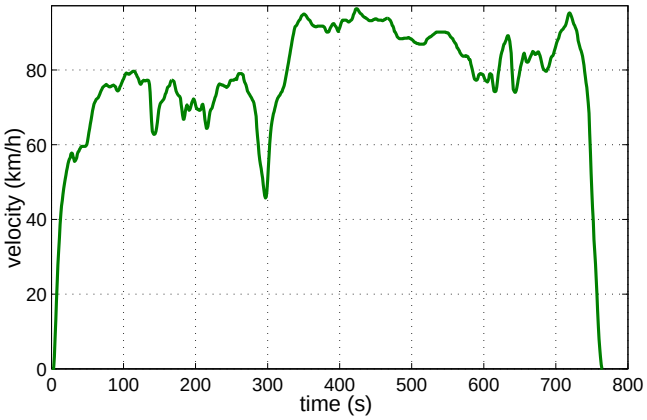


Figure 4.4: HWFET drive cycle

We selected the EPA (Environmental Protection Agency) drive cycle (Figure 4.5) to represent combined urban and highway driving cycles. EPA drive cycle characteristics are given in Table 4.4.

Table 4.4: EPA characteristics

| Description | Value |
|---|---|
| $TotalTime$ | $2135s$ |
| $Distance$ | $28.5km$ |
| $AverageSpeed$ | $54.8km/h$ |
| $MaxSpeed$ | $96.4km/h$ |
| $MaxAcceleration$ | $1.47m/s^2$ |

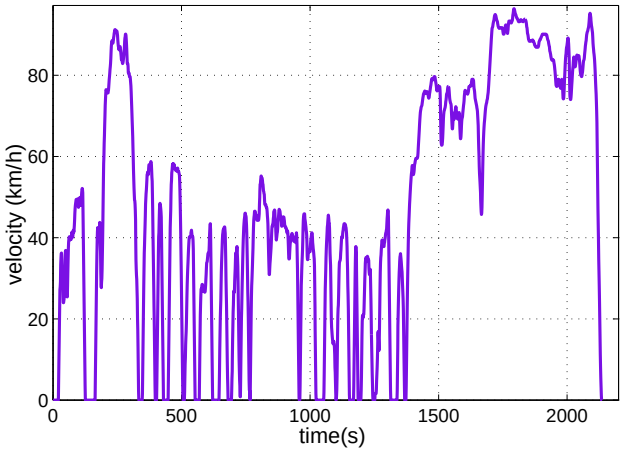


Figure 4.5: EPA drive cycle

To calculate fuel economy for combined city and highway driving patterns, according to the equation 4.1 [12,35,37] a composite fuel economy can be obtained by combining the highway and city fuel consumption:

$$CompositeFuelEconomy = \frac{1}{0.55/City\_FE + 0.45/Hwy\_FE} \tag{4.1}$$

where $City\_FE$ and $Hwy\_FE$ represent the city and highway fuel economy values, respectively.

## 4.6 Simulation in Autonomie

Before running the optimization and sizing of the components, we simulated the base model (Prius 2012) in Autonomie based on the specifications given in Chapter 3 and using the EPA drive cycle. This method allowed us to obtain the behaviour of the model, which can be compared against the optimization results later on.

Figure 4.6 depicts the difference between the real speed of the vehicle and the drive cycle. As it can be seen, the vehicle could closely track the drive cycle.

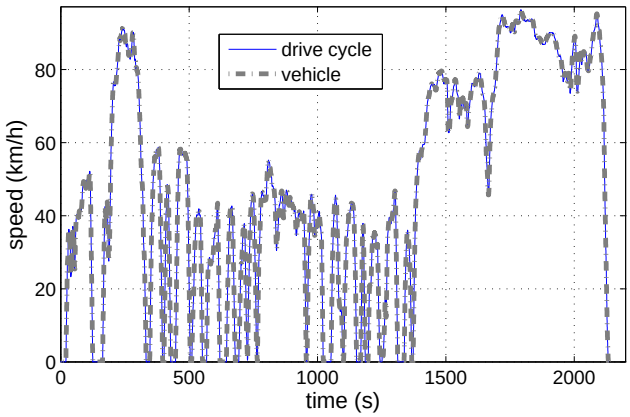


(a) the vehicle tracking the drive cycle

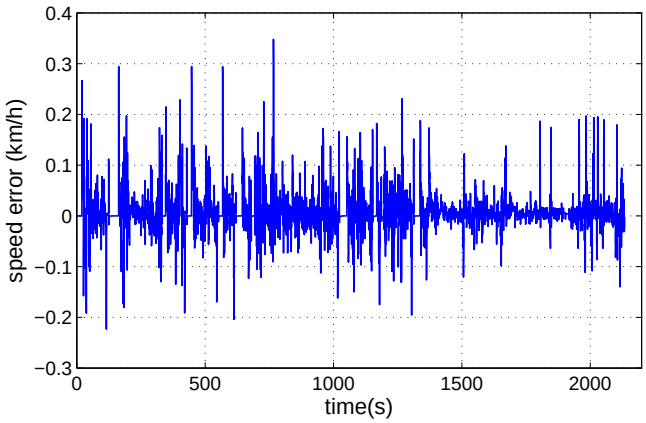


(b) speed difference

Figure 4.6: Tracking the EPA cycle

Power distributions between the powertrain components are depicted in Figures 4.7 through 4.10.

It is clear from Figure 4.7 that the engine mostly propelled the vehicle while in charge sustaining mode. The engine also turned on when power demands were high, even if the battery $SOC$ was higher than the target (0.3) [46]. According to the power-split

configuration, the generator worked when the engine turned on in order to bring it to its optimum working points (Figure 4.8).

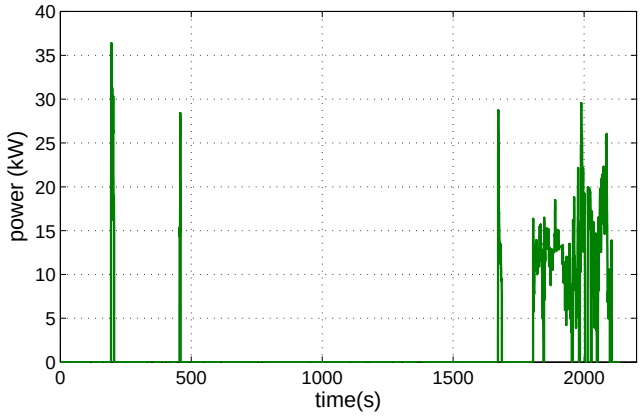


Figure 4.7: Engine and battery power in EPA cycle

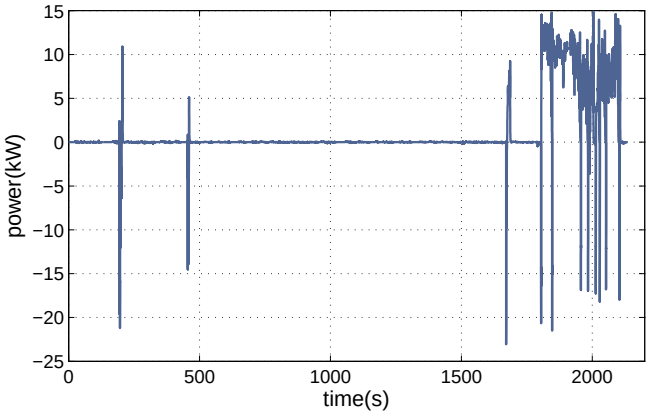


Figure 4.8: Generator power in EPA cycle

Figures 4.9 and 4.10 show that the battery provided the primary propulsion power for the vehicle until it reached its target $SOC$. As a result, the motor power (Figure 4.10) is

similar to the battery power.

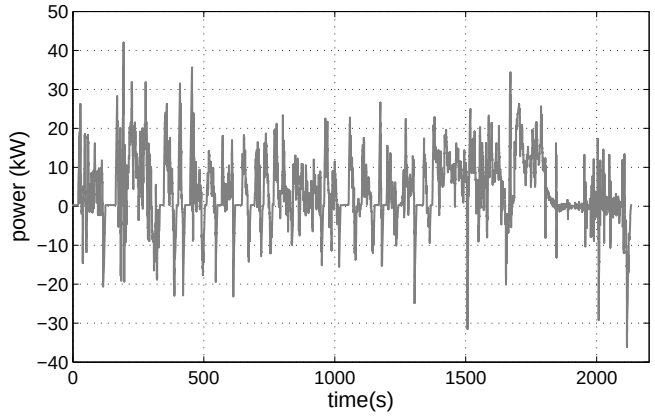


Figure 4.9: Battery power in EPA cycle

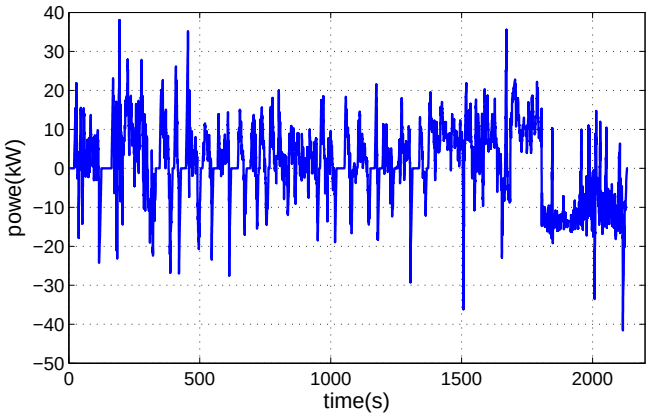


Figure 4.10: Motor power in EPA cycle

## 4.7 Two Variable Optimization

We started optimization with two design variables, maximum engine and electric motor power. The results, taking into consideration the boundary conditions (Table 4.5), show that the engine and motor were both downsized; however, the reduction in the engine size is more considerable. The downsized engine and motor can easily provide the power required for the EPA cycle. Optimization completed without considering the performance constraints resulted in downsized motor and engine components. This is due to the fact that the power demands in typical driving patterns such as EPA are lower than the required power for desired performances. Engines and motors with small sizes can easily provide these powers (final value in Table 4.5).

Table 4.5: Two variable optimization results

| Design variable | Lower bound | Upper bound | Default value | Final value |
|---|---|---|---|---|
| $P_e$ | $30kW$ | $100kW$ | $73kW$ | $33.66kW$ |
| $P_m$ | $10kW$ | $70kW$ | $60kW$ | $23.07kW$ |

As mentioned earlier, during the optimization, the vehicle weight was adjusted as the engine and motor sizes were optimized.

## 4.8 Three Variable Optimization

Initially, the optimization ran with two variables, but given the important role batteries play in PHEV platforms, it was important to obtain optimal batteries sizing in addition to engine and motor sizes.

Therefore, before running the optimization for this case, the boundaries for the battery were determined. The minimum boundary for the number of battery cells was calculated based on the voltage ratio between the battery and the electric motor [29]:

$$N_{b-min} = \frac{V_m}{V_b} \tag{4.2}$$

where $V_m$ and $V_b$ represent the minimum voltage of the motor and battery cell (120 and $3.7V$, respectively). Thus, the minimum boundary for the third design variable was 32 battery cells.

Consequently, the optimization was carried out again, this time adding the number of battery cells as the third design variable. No change in the objective and constraints of the two variable optimization were set. The only difference was that in optimization with the engine and electric motor sizes as the design variables, the mass of optimized design parameters were adjusted but in this case changing in mass of battery cells were not considered. In detail, during this optimization the number of battery cells, $N_b$, would get a different value from 32 to 68. According to Toyota document, the mass of each li-ion cell in Prius is about 700 grams [43], this would not have a significant effect on the fuel consumption of the vehicle. So the vehicle mass were adjusted only with adjustment in the

engine and electric motor masses. The change in battery mass due to different $N_b$ were not taken into consideration.

The battery sizing optimization results went toward the maximum allowed battery cells (68, Table 4.6). This can be explained by the fact that in the PHEV, the battery propels the vehicle until it reaches its target $SOC$ (0.3 for our model) beyond which the engine drives the vehicle and charges the batteries. Therefore, by increasing the number of battery cells, the vehicle would mostly run by the electric power. As a result, the higher number of batteries leads to lower fuel consumption. So, the optimization called for the largest possible number of batteries in order to minimize fuel consumption.

Table 4.6: Optimization results for 3 design variables

| Design variable | Lower bound | Upper bound | Default value | Final value |
|---|---|---|---|---|
| $P_e$ | $30kW$ | $100kW$ | $73kW$ | $30kW$ |
| $P_m$ | $10kW$ | $70kW$ | $60kW$ | $56.7kW$ |
| $N_b$ | 32 | 68 | 56 | 68 |

To solve the above mentioned problem, we could assume that the initial and final $SOC$ of the battery are the same (charge-depleting charge-sustaining mode). Based on this assumption, the engine would mainly run the vehicle. However, this would result in the vehicle working like a HEV, which was not the case. Therefore, an alternative solution had to be found. Changing the objective could be helpful in this regard.

## 4.9 Multi-Objective Optimization

Another way to obtain a reasonable optimization result for the number of battery cells is to consider the cost of electricity in the objective function. This is particularly germane since our model is a PHEV that can be charged by connecting to the grid. For this purpose, the objective function was changed and defined in terms of cost of operating fuels. So minimizing the gasoline consumption was no longer the primary interest, instead the optimization would address both the optimum the cost of electricity and minimized gasoline consumption as the new objectives. As a result, the single term objective function turned to the following form:

$$J = C_f \times m_f + C_e \times E_b \times N_b \tag{4.3}$$

where $C_f$ is the cost of gasoline per litre ($\$/litre$), $m_f$ is the gasoline consumption for each drive cycle (litre), $C_e$ is the electricity cost ($\$/kWh$)for each drive cycle, $E_b$ is the electricity consumption for each drive cycle in $kWh$, and $N_b$ is the total number of battery cells. $1.2\$/litre$ and $0.1\$/kWh$ were assumed for the unit cost of gasoline and electricity, respectively. These are the approximate values for Canada in the past year [62, 63].

Being more precise, we can also consider the cost of battery maintenance in the above objective function. For this purpose, battery maintenance cost would be added to the objective function in the form:

$$J = \frac{\text{cost of each battery cell}}{\text{battery life time}} \times N_b \tag{4.4}$$

The approximate daily battery cost assuming the cost of 80\$/*cell* [64] and a 10 year life time for the battery, yields:

$$J = \frac{120}{10 \times \gamma} \times (N_b) \tag{4.5}$$

where $\gamma$ in the above equation is defined as the number of cycles per year.

We assumed that the vehicle drives 20000 $km$ per year. As a result considering the EPA driving distance(Table4.4), $\gamma$ would be 701.75 for EPA drive cycle. Consequently, following equation 4.3 to 4.5, the cost function for the EPA drive cycle would be:

$$J = 1.2 \times m_f + 0.1 \times E_b \times (N_b) + \frac{80}{10 \times 701.75}(N_b) \tag{4.6}$$

The optimization with this cost function and for about 400 evaluations (Figure 4.11) resulted in the downsizing of all three target components with respect to their default values. As was the case when optimizing two variables, this downsizing is due to the fact that we did not consider any performance constraints (except the drive cycle requirements) in these optimizations. Therefore, without constraints, the algorithm tended toward a cheaper battery cost and lesser fuel consumption, which yielded a smaller engine, motor and battery. However, in comparison with the two-variable optimization, the engine was oversized, while the electric motor was downsized. Fewer battery cells (Table 4.7)compared to the default model can be the reason for getting the smaller size engine.

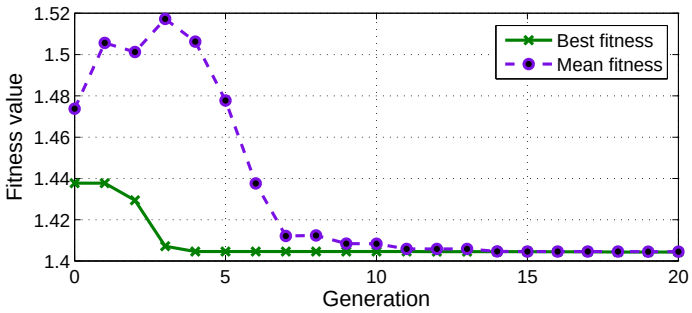


Figure 4.11: GA results for three variable optimization regarding cost in EPA cycle

In the above figure, the fitness value is the value of the objective function at each generation. 20 generations were considered as the end criteria for GA. The mean fitness reveals the progress of the algorithm. This means that at each generation we would get a new mean fitness due to changes in the population. This continues until the average reaches the best fitness, which is the most desirable outcome.

Table 4.7: Multi-objective optimization results for 3 design variables

| Design variable | Final value |
|---|---|
| $P_e$ | $41.3kW$ |
| $P_m$ | $19.34kW$ |
| $N_b$ | 42 |

## 4.10 Performance Constraints

As mentioned in the previous section, the large differences seen between the design variables and their default values in the model are the result of not taking any constraints into account in the sizing optimization. Thus, in order to ensure that our optimized component sizes can not only meet cost and fuel consumption objectives but also fulfill certain vehicle performance requirements, some constraints were added as boundary conditions to the optimization process and the optimization was carried out again. This is helpful in preventing the GA algorithm from selecting low design variables.

The main vehicle performance constraints relate to grading, cruising, and accelerating to a specific speed within a desired time limit. Cruising with constant speed at full power will give the maximum vehicle speed, which can be used to calculate the power required from the powertrain to reach this speed. Therefore, according to equations 3.2 and 3.10, we have:

$$P_{cruise} = V(mg\sin\alpha + \frac{1}{2}C_D V^2 + C_r mg\cos\alpha) \tag{4.7}$$

In this calculation, the acceleration term has been omitted due to the constant speed. The values for the parameters were taken from Table 3.1 in the modeling chapter. The road grade $\alpha$ is set to zero. Consequently, the powertrain should provide sufficient power ($95.6kW$) to reach the maximum speed of $180km/h$. The electric motor and engine should provide this power together. Therefore, we assumed that the total minimum power of these two power supplies should be equal to the power required for the maximum speed.

Gradability, as another important vehicle performance constraint, was considered to

calculate the minimum engine power. From equation 4.7, $45kW$ power required a 5% grade with constant speed of 100 $km/h$. Assuming a 90% efficiency for the powertrain, the minimum engine power would be about $50kW$. Therefore, to achieve the maximum speed of $180km/h$, the electric motor requires a minimum power of $46kW$.

Another criterion to verify the performance of a vehicle is acceleration time. As explained in the previous chapter, an acceleration time less than 12 seconds for 0 to $60mph$ is desired according to PNGV consortium goals. We considered this acceleration time as another performance constraint for the vehicle and optimization process in general and calculated the power required for this constraint as [65]:

$$P = \frac{\delta m}{2t}(V_f^2 + V_b^2) + \frac{2}{3}mgC_rV_f + \frac{1}{5}\rho AC_DV_f^3 \tag{4.8}$$

where $V_f$ and $\delta$ are the final acceleration speed and mass factor respectively. The second and third terms in the above equation are the power required for rolling resistance and drag, and the corresponding parameter and coefficients are defined based on values given in Chapter 3. $V_b$, the vehicle base speed, can be calculated from [27, 65]:

$$V_b = \frac{\pi\omega_b R}{30K_{fd}} \tag{4.9}$$

In the above equation, $\omega_b$, the rotational speed at constant torque, was obtained from the motor torque map based on speed (Figure 4.12) and is equal to $1250rpm(131rad/s)$. With $K_{fd}$, the final drive ratio would equal to 4.113, the base speed would be $9.55m/s$.

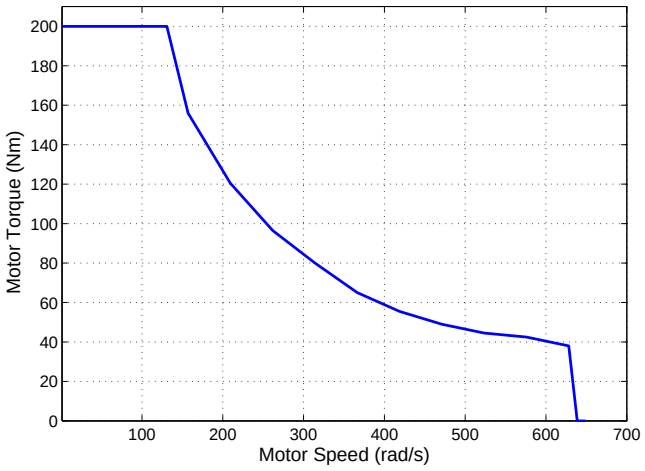


Figure 4.12: Torque versus speed

The unit-less mass factor $\delta$, which is due to the rotating components, can be obtained from the following equation [65]:

$$\delta = 1 + \delta_1 + \delta_2 K_{fd}^2 \tag{4.10}$$

where $\delta_1$ is associated with the moment of inertia of the wheels with an estimated value of 0.04, $\delta_2$ is due to the rotating components of powertrain with an estimated value of 0.0025. Therefore, the value for $\delta$ would be 1.046 [65].

As a result, based on equation 4.8 and the corresponding values, a power of about $70kW$ is required to accelerate from 0 to $100km/h$ in less than 12 seconds. This power is less than the power required to reach the maximum speed ($95.6kW$). So the latter is used to find the minimum power required for the motor to satisfy all of the above constraints.

The minimum engine power required to satisfy the gradability conditions was found to be about $50kW$. As a result the minimum power of about $45kW$ for the electric motor was obtained.

Therefore, optimization was run again, this time taking into account the performance constraints since the minimum boundaries for the design variables were determined with respect to them. The GA for this case converged very quickly to the fittest value, before it reached 10 generations (Figure 4.13).

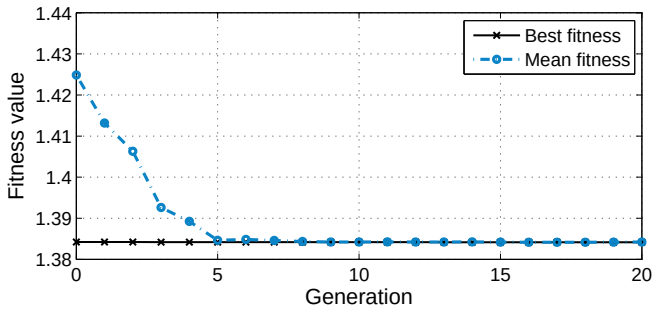


Figure 4.13: GA results for 3 variable constrained optimization with respect to cost in EPA cycle

Results for the EPA cycle (Table 4.8) show that except for the battery, the engine and motor were both downsized with respect to their values in the base model. However, a comparison between these results and those without constraints (Table 4.7) illustrates the fact that a better performance led to increased component sizes, which conflicts with the fuel consumption objective.

Table 4.8: Multi-objective optimization results for 3 design variables considering performance constraints

| Design variable | Final value | Size variation(%) |
|---|---|---|
| $P_e$ | $52.3kW$ | -28.4 |
| $P_m$ | $49.2kW$ | -18 |
| $N_b$ | 62 | +10.7 |

We repeated the constrained optimization with two and three design variables, and fuel consumption as the single objective. When three design variables were considered, the GA (Figure 4.14) approached the best fitness after almost 10-12 generations.

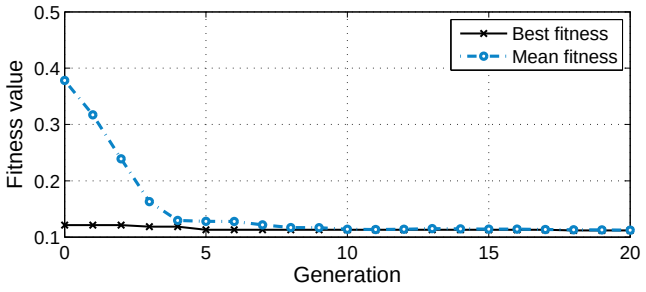


Figure 4.14: GA results for 3-variable constrained optimization to minimize fuel consumption in the EPA cycle

The optimization results for the component sizes (Table 4.9) show that when the cost of electricity does not matter, a larger size of motor and battery would be more desirable as it may be more helpful in reducing fuel consumption because a larger portion of the power demand would be provided by these components. This shows that increase in size of the

components and in general the vehicle mass did not have a big effect on fuel consumption.

Table 4.9: Optimization results with objective of minimizing fuel consumption and considering performance constraints

| Design variable | Final value | |
|---|---|---|
| | 2 variables | 3 variables |
| $P_e$ | $53.6kW$ | $52kW$ |
| $P_m$ | $69kW$ | $52kW$ |
| $N_b$ | - | 68 |

The fuel consumption results for all 6 sets of optimizations are classified in the table below to provide a general view of the results and facilitate an easy comparison.

Table 4.10: Fuel consumption results for EPA

| | Constraints | Number of Variables | Objective | Fuel Consumption ($l/100km$) |
|---|---|---|---|---|
| 1 | + | 3 | total cost | 1.073 |
| 2 | − | 3 | total cost | 2.039 |
| 3 | + | 3 | fuel consumption | 0.525 |
| 4 | + | 2 | fuel consumption | 1.156 |
| 5 | − | 3 | fuel consumption | 0.492 |
| 6 | − | 2 | fuel consumption | 1.078 |

As can be seen, in the first two sets, where optimizations were done in terms of total

cost, the premier with constrained optimization has a lower fuel consumption due to its larger battery pack, although it has a bigger engine to satisfy the performance constraints.

In the next two sets (3 and 4), the optimizations were run with constraints and with the objective of minimizing fuel consumption. The fourth optimization produced a higher fuel consumption rate because it had fewer battery cells; the relevant optimization was with two variables and the number of batteries were fixed and was the same as in the base model. The third optimization had the maximum allowable number of battery cells (a third design variable optimization) and demonstrated the lowest fuel consumption to this point.

The fifth and sixth sets were again optimized to meet the fuel consumption objective, but without considering performance constraints. The fifth set provided the best result in achieving the lowest fuel consumption. This was due to the maximum battery size and the minimum engine size.

The comparison between optimizations undertaken with and without constraints, whether considering two or three design variables, showed that the latter produced worse results in fuel consumption. This was expected because of the fewer number of batteries, which led more power producing by the engine and consequently higher fuel consumption.

## 4.11 Comparison Between the Base Model and Optimization Results

In order to assess our component size optimization results, we compared our model's fuel consumption results against those derived from the base model.

The error value in Table 4.11 reveals the comparison between fuel consumption results before optimization ($1.26l/100km$) and after (Table 4.10) for the EPA cycle.

Table 4.11: Fuel consumption comparison before and after optimization

| | Constraints | Number of Variables | Objective | Difference(%) |
|---|---|---|---|---|
| 1 | + | 3 | total cost | 14.43 |
| 2 | − | 3 | total cost | -89.75 |
| 3 | + | 3 | fuel consumption | 58.37 |
| 4 | + | 2 | fuel consumption | 8.21 |
| 5 | − | 3 | fuel consumption | 60.94 |
| 6 | − | 2 | fuel consumption | 14.8 |

Figure 4.15 provides fuel consumption plots with default component sizes and obtained component sizes from constrained optimization with both fuel consumption and cost objectives. As expected, sizing optimization to address the fuel consumption objective produced the lowest consumption. According to the power distribution described earlier, the fuel consumption in all three results increased when the CS mode was initiated and the engine

turned on.

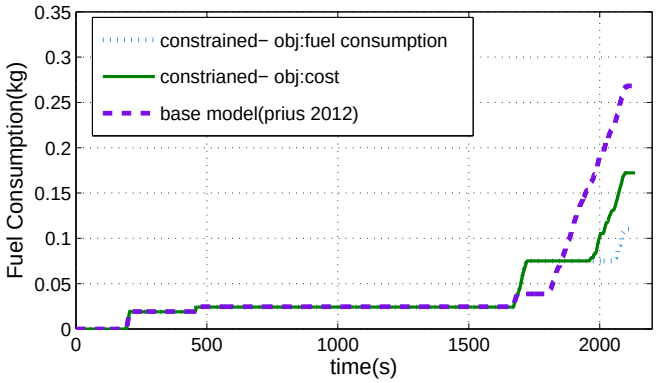


Figure 4.15: Fuel consumption plots for 3-variable constrained optimization and the base model

Figure 4.16 depicts the *SOC* behaviour of the battery during the EPA cycle for the model before and after sizing. In all three plots, *SOC* depleted from 90 percent and finally reached the minimum level of 30 percent; however, the time and rate of depletion differs across optimization results.

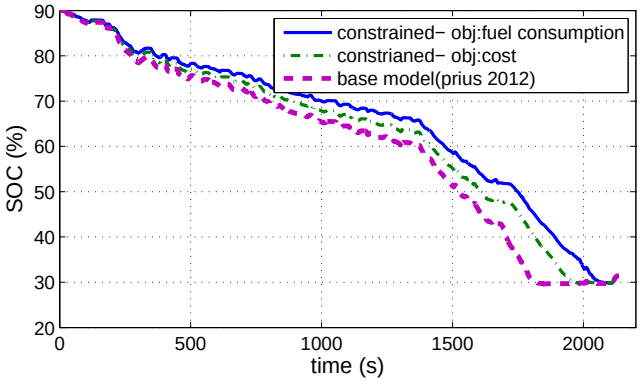


Figure 4.16: SOC for 3-variable constrained optimization and the base model

In accordance with the governing performance constraints, it was expected that the time of less than $12s$ to accelerate from $0 - 60mph$ $(96Km/h)$ would be achieved in the simulation with the optimization results; Table 4.12 clearly shows that this was indeed the case. Figure 4.17 shows the acceleration cycle for the three cases in Table 4.12.

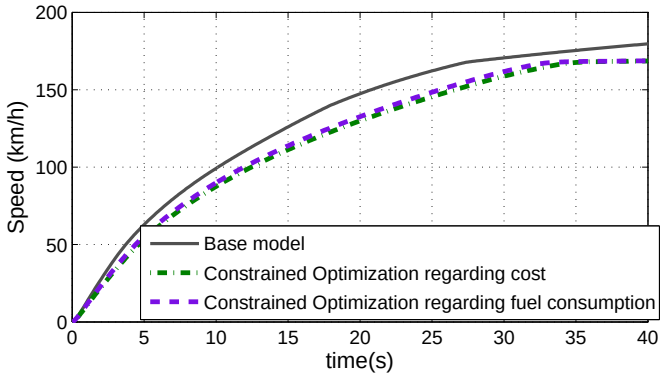


Figure 4.17: Acceleration speed for 3-variable constrained optimization and the base model

Table 4.12: Acceleration results

| Description | Acceleration time (s) |
|---|---|
| Base model | 9.4 |
| Constrained 3 variable optimization regarding fuel consumption | 11.1 |
| Constrained 3 variable optimization regarding cost | 11.6 |

Although lower fuel consumption rates were achieved by downsizing the main components, Table 4.12 reveals that the base model has a better performance in comparison with the optimization results. However, this trade-off always exists between performance and fuel cost; which benefit is preferred depends on the target objective.

## 4.12 Optimization with FTP Drive Cycle

To this point, the optimization results were carried out for the EPA cycle, which is a combination of city and highway cycles. In order to consider the sizing for urban and highway cycles individually, we ran the optimizations again for the FTP cycle, described in this section, and HWFET, described in the next section.

In the case of sizing to achieve minimized fuel consumption, we ran optimizations with and without constraints for two and three design variables for the FTP cycle (2 times).

Table 4.13: Optimization results for 2 and 3 design variables for FTP

| Design variable | with constraint | | without constraint | |
|---|---|---|---|---|
| | 2 variables | 3 variables | 2 variables | 3 variables |
| $P_e$ | $50kW$ | $54.9kW$ | $36.4kW$ | $41kW$ |
| $P_m$ | $58.3kW$ | $68.3kW$ | $29.8kW$ | $29.4kW$ |
| $N_b$ | - | 68 | - | 68 |

The results (Table 4.13) are completely justifiable. Adding the performance constraints to the optimization led to increased component sizes. When the number of battery cells was added as a third design variable, the optimization results went toward integrating the maximum possible number of batteries to minimize fuel consumption.

In another attempt, we changed the optimization objective and tracked the effect of cost on the sizing of the components, again with and without performance constraints. The results were as follows:

Table 4.14: Multi-objective optimization results for FTP

| Design variable | with constraint | without constraint |
|---|---|---|
| $P_e$ | $48.89kW$ | $30.12kW$ |
| $P_m$ | $60.58kW$ | $23.07kW$ |
| $N_b$ | 49 | 39 |

The fuel consumption results for all optimizations carried out for this drive path are given in Table 4.15. In general, if we compare the fuel consumption results for this cycle with those for the EPA cycle (Table 4.10), without exception, the former one produced higher consumption rates in all cases. This obviously could be because of the difference in the driving cycle. As an urban cycle, the FTP path requires more fuel consumption due to its stop and go pattern.

Table 4.15: Fuel consumption results for FTP

| | Constraints | Number of Variables | Objective | Fuel Consumption ($l/100km$) |
|---|---|---|---|---|
| 1 | + | 3 | total cost | 2.591 |
| 2 | − | 3 | total cost | 2.039 |
| 3 | + | 3 | fuel consumption | 1.143 |
| 4 | + | 2 | fuel consumption | 1.661 |
| 5 | − | 3 | fuel consumption | 1.094 |
| 6 | − | 2 | fuel consumption | 1.582 |

In the above table, the optimization results listed in the first and second row were run with respect to cost. The first optimization has a lower fuel consumption result due to a larger size battery. The second one has smaller size engine and motor; however, this had little benefit to fuel economy since the objective function cares more about the total cost than fuel consumption solely.

Considering the optimizations undertaken to minimize fuel consumption, and with constraints considered, the three variable one (third row) shows a better result because its larger battery would take over the role of propelling the vehicle to save fuel.

The last two optimization results did not consider performance constraints and therefore achieved the minimum fuel consumption (fifth row) with the maximum number of battery cells and minimum sized engine and motor components. Table 4.16 summarizes a fuel consumption comparison before and after optimization with FTP as a drive cycle.

Table 4.16: Fuel consumption comparison before and after optimization

| | Constraints | Number of Variables | Objective | Difference(%) |
|---|---|---|---|---|
| 1 | + | 3 | total cost | -70.72 |
| 2 | − | 3 | total cost | -110.71 |
| 3 | + | 3 | fuel consumption | 44.22 |
| 4 | + | 2 | fuel consumption | 3.1 |
| 5 | − | 3 | fuel consumption | 48.06 |
| 6 | − | 2 | fuel consumption | 9.32 |

## 4.13 Optimization with HWFET Drive Cycle

The same processes described above were carried out for the HWFET drive cycle. The results are given below:

Table 4.17: Optimization results for 2 and 3 design variables for HWFET

| Design variable | with constraint | | without constraint | |
|---|---|---|---|---|
| | 2 variables | 3 variables | 2 variables | 3 variables |
| $P_e$ | $53.41kW$ | $50kW$ | $31kW$ | $43.76kW$ |
| $P_m$ | $74.67kW$ | $78.56kW$ | $31kW$ | $23.13kW$ |
| $N_b$ | - | 68 | - | 68 |

Re-running the optimization by changing the objective function to address cost, yielded:

Table 4.18: Multi-objective optimization results for HWFET

| Design variable | with constraint | without constraint |
|---|---|---|
| $P_e$ | $50kW$ | $30kW$ |
| $P_m$ | $51.28kW$ | $18.74kW$ |
| $N_b$ | 35 | 32 |

Fuel consumption results for this cycle are given in Table 4.19. With exception of the cases with cost as the objective, a reasonable reduction in fuel consumption can be seen considering the base model consumption with this cycle is $1.84l/100km$

Table 4.19: Fuel consumption results for HWFET

| | Constraints | Number of Variables | Objective | Fuel Consumption ($l/100km$) |
|---|---|---|---|---|
| 1 | + | 3 | total cost | 3.497 |
| 2 | − | 3 | total cost | 2.67 |
| 3 | + | 3 | fuel consumption | 1.155 |
| 4 | + | 2 | fuel consumption | 1.7 |
| 5 | − | 3 | fuel consumption | 1.102 |
| 6 | − | 2 | fuel consumption | 1.586 |

Table 4.20 provides a comparison of fuel consumption rates before and after optimization with HWFET cycle.

Table 4.20: Fuel consumption comparison before and after optimization

| | Constraints | Number of Variables | Objective | Difference(%) |
|---|---|---|---|---|
| 1 | + | 3 | total cost | -90.04 |
| 2 | − | 3 | total cost | -45.12 |
| 3 | + | 3 | fuel consumption | 37.24 |
| 4 | + | 2 | fuel consumption | 7.67 |
| 5 | − | 3 | fuel consumption | 40.1 |
| 6 | − | 2 | fuel consumption | 13.8 |

## 4.14 Summary

This chapter summarized and compared optimization results for different driving cycles, considering 2 and 3 design variables, with and without constraints, and both fuel consumption and cost objectives. Considering results provided in Tables 4.10, 4.15 and 4.19, in general the EPA cycle revealed better results in most cases and a desirable reduction of fuel consumption was achieved.

In the EPA drive cycle, component sizing to address cost, and with three design variables considered, resulted in the lowest fuel consumption rate by comparison with all the optimization results (Tables 4.10 and 4.11). This was largely due to reaching the maximum possible number of batteries in the resulting configuration. When performance constraints were not considered, these results showed an even deeper reduction in fuel consumption.

In general, among the six modes of optimization done for the EPA cycle (Tables 4.5 to 4.9), the engine was downsized with respect to its initial size. This is also true for the motor except when two design variables performance constraints were considered (Table 4.9), and where the number of batteries were fixed and equal to the initial value. In this case, the engine reached its maximum size with respect to the other five cases. The number of batteries could increase and as a result the motor had to be oversized to meet the performance requirement. Battery sizes were fixed or oversized in most of the cases, except when the cost was the objective (indicating larger size batteries would be costly). Clearly the minimum size for the components was obtained when performance constraints were not considered.

Similarly, in the optimization using the FTP drive cycle, the minimum fuel consumption

was found when three design variables were considered and the objective was minimized fuel consumption, whether with or without constraints (Table 4.15). With a maximum battery size and downsized engine and motor components, reduced fuel consumption was achieved. Again, the minimum sized battery was achieved when cost was the objective, which is obvious when the cost of the battery is considered in addition to fuel cost. The engine size was reduced significantly in all cases. This was also the case for the motor when there were no constraints on the optimization (Tables 4.13 and 4.14). The maximum size for the engine, motor and battery were obtained during the optimization with fuel consumption as the objective and where performance constraints were considered (Table 4.13).

According to Table 4.19, the minimum fuel consumption for HWFET cycle, likewise the other two drive cycles (EPA and FTP), was achieved when three design variables were considered and fuel consumption was the design objective. Again, the engine was downsized in all cases, while the motor had a lager size than its initial design when constraints were placed on the optimization and fuel consumption was the objective (Table 4.17). By comparison with the FTP results, the battery size with this cycle was extremely downsized when cost was the objective. This is due to the fact that FTP, as an urban cycle, would require larger battery.

# Chapter 5

# Conclusion and Future work

## 5.1 Conclusion

In this research project, we developed a power-split PHEV model based on the Toyota Prius platform model. Autonomie was used as a simulation tool to support development of the vehicle model, which was evaluated before running the optimization to determine the effect of sizing on fuel consumption and vehicle performance. Based on this analysis, we were able to validate the optimization results beforehand. Using this model, an optimization problem was formulated to minimize fuel consumption, our primary objective. We were able to find optimized sizes for key components of the vehicle, including the engine, electric motor, and batteries. Thus, engine and motor maximum power, and the number of battery cells were our primary design variables. The Genetic Algorithm (GA) approach was employed as the optimization algorithm, and the problem was solved for various drive cycles, including

urban, highway, and a combination of both.

Based on this component sizing effort, a significant reduction in fuel consumption achieved by comparison with rates derived from the initial model and in different drive cycles, whether urban (FTP) or highway (HWFET) or a combination of urban and highway cycles (EPA). Although some of our optimization results, found without considering constraints, showed significantly reduced fuel consumption, the resulting vehicle platform could not meet required performance criteria and were therefore undesirable.

In this research project, we integrated Autonomie PHEV models and GA optimization to create a framework that can be used to address any optimization problem to meet any objective, constraint, design variables and optimization parameters.

We can derive several conclusions from this research, including:

- Finding optimized powertrain component sizing can lead to significant reductions in fuel consumption.
- Fuel consumption rates are tightly linked to the driving cycle considered. This was validated in Chapter 4, which directly evaluated the effects of urban, highway, and combined driving cycles on fuel consumption.
- Fuel consumption results vary considerably depending on whether performance constraints are or are not taken into account. This demonstrates the close interconnection between fuel consumption and performance constraints, suggesting they should always be taken into account.

- Going forward, the objective function should be modified to include the total cost of battery maintenance and fuel consumption. Optimal sizing for the powertrain components to minimize cost were derived. This process was repeated for different drive cycles and took the performance constraints into account. The influence of drive cycle and performance on fuel consumption followed the same trend as described earlier, although fuel consumption results are much higher with total cost as the objective.

## 5.2 Future Work

The following can be considered for continuation of this research:

- Optimization can be developed by considering more design parameters including other powertain parameters (such as $f_d$ ratio) and the controller parameters (such as $SOC_{min}$).

- More objectives can be considered in the optimization such as emission or the total cost of vehicle.

- Rather than GA, other alternative Optimization approaches can be utilized such as global optimization methods (like PSO, DP, ...) or integrating GA with a gradient-based method and obtain a robust algorithm. The results of different optimization algorithms can be compared.

# References


[1] S. Golbuff, "Design optimization of a plug-in hybrid electric vehicle," *SAE Technical Papers*, 04 2007.

[2] J. Zeman and I. Papadimitriou, "Modeling and optimization of plug-In hybrid electric vehicle fuel economy," *SAE Technical Papers*, 2012.

[3] T.-S. Dao, A. Seaman, J. McPhee, and K. Shigematsu, "Development of a high-fidelity series-hybrid electric vehicle model using a mathematics-based approach," *SAE International*, no. 9, 2012.

[4] F. Mapelli, M. Mauri, and D. Tarsitano, "Plug-in hybrid electrical commercial vehicle: modeling and prototype realization," pp. 1–8, Mar. 2012.

[5] F. Cheli, F. L. Mapelli, R. Manigrasso, and D. Tarsitano, "Full energetic model of a plug-in hybrid electrical vehicle," in *SPEEDAM - International Symposium on Power Electronics, Electrical Drives, Automation and Motion*, pp. 733–738, Ieee, June 2008.

[6] Z. Fu, G. Hou, and A. Gao, "Modeling and simulation for parallel hybrid electric vehicle powertrain," in *Advanced Mechatronic Systems (ICAMechS), 2011 International Conference on*, pp. 114–117, 2011.

[7] M. Cipek, D. Pavkovi, and J. Petri, "A control-oriented simulation model of a power-split hybrid electric vehicle," *Applied Energy*, vol. 101, pp. 121 – 133, 2013.

[8] J. Ahn, K. Jung, D. Kim, H. Jin, H. Kim, and S. Hwang, "Analysis of a regenerative braking system for hybrid electric vehicles using an electro-mechanical brake," *International Journal of Automotive Technology*, vol. 10, no. 2, pp. 229–234, 2009.

[9] Y. Ye, Y. Shi, N. Cai, J. Lee, and X. He, "Electro-thermal modeling and experimental validation for lithium ion battery," *Journal of Power Sources*, vol. 199, pp. 227 – 238, 2012.

[10] S. Williamson, A. Emadi, and K. Rajashekara, "Comprehensive efficiency modeling of electric traction motor drives for hybrid electric vehicle propulsion applications," *IEEE Transactions on Vehicular Technology*, vol. 56, no. 4, pp. 1561–1572, 2007.

[11] P. C. Manning, E. White, R. J. Alley, J. King, and D. J. Nelson, "Vehicle system design process for a series-parallel plug-in hybrid electric vehicle," *SAE International Journal of Alternative Powertrains*, vol. 1, no. 2, pp. 503–524, 2012.

[12] D. W. Gao, C. Mi, and A. Emadi, "Modeling and simulation of electric and hybrid vehicles," *Proceedings of the IEEE*, vol. 95, pp. 729–745, Apr. 2007.

[13] Y. Ma, H. Teng, and M. Thelliez, "Electro-thermal modeling of a lithium-ion battery system," *SAE International Journal of Engines*, vol. 3, no. 2, pp. 306–317, 2010.

[14] X. Hu, S. Lin, S. Stanton, and W. Lian, "A state space thermal model for HEV/EV battery modeling," *SAE paper*, 2011.

[15] E. C. De Oliveira and D. C. Donha, "Modeling and Simulation of Small Hybrid," *SAE Technical Papers*, 2006.

[16] K. Butler, M. Ehsani, and P. Kamath, "A Matlab-based modeling and simulation package for electric and hybrid electric vehicle design," *IEEE Transactions on Vehicular Technology*, vol. 48, no. 6, pp. 1770–1778, 1999.

[17] X. He, "Battery Modeling for HEV Simulation Model Development," *SAE paper*, no. 724, 2001.

[18] H. Zhang and M. . Chow, "Comprehensive dynamic battery modeling for phev applications," in *IEEE Power and Energy Society General Meeting*, pp. 1–6, IEEE, 2010.

[19] X. He and J. Hodgson, "Modeling and simulation for hybrid electric vehicles. i. modeling," *IEEE Transactions on Intelligent Transportation Systems*, vol. 3, no. 4, pp. 235–243, 2002.

[20] W. Gao and S. Porandla, "Design optimization of a parallel hybrid electric powertrain," *Vehicle Power and Propulsion Conference,VPPC*, pp. 530–535, 2005.

[21] J. Deur, M. Cipek, and J. Petrić, "Bond graph modeling of series-parallel hybrid electric vehicle power train dynamics," in *Proceedings of the 2010 Spring Simulation Multiconference*, SpringSim '10, pp. 218:1–218:10, Society for Computer Simulation International, 2010.

[22] E. Tara, S. Shahidinejad, S. Filizadeh, and E. Bibeau, "Battery storage sizing in a retrofitted plug-in hybrid electric vehicle," *IEEE Transactions on Vehicular Technology*, vol. 59, no. 6, pp. 2786–2794, 2010.

[23] C. Musardo, G. Rizzoni, Y. Guezennec, and B. Staccia, "A-ECMS: An adaptive algorithm for hybrid electric vehicle energy management," *European Journal of Control*, vol. 11, pp. 509–524, Oct. 2005.

[24] S. Hamidifar and N. Kar, "Energy based graphical user interface modeling for PHEV energy management system," *Electrical Power & Energy Conference (EPEC)*, pp. 1–6, 2009.

[25] J. Che, P. Tsou, L. Rose, and M. Jennings, "Modeling and simulation of the dual drive hybrid electric propulsion system," *SAE Technical Papers*, 2009.

[26] J. Batteh and M. Tiller, "Implementation of an extended vehicle model architecture in modelica for hybrid vehicle modeling: development and applications," *Proceedings 7th Modelica Conference*, pp. 823–832, Oct. 2009.

[27] A. H. Niasar, H. Moghbelli, and A. Vahedi, "Design methodology of drive train for a series-parallel hybrid electric vehicle (sp-hev) and its power flow control strategy," in *International Conference on Electric Machines and Drives*, pp. 1549–1554, IEEE, 2005.

[28] S. Overington, S. Rajakaruna, and S. Member, "A modified method for the sizing of the plug-in hybrid electric vehicle propulsion devices," *Universities Power Engineering Conference (AUPEC)*, pp. 1–7, 2011.

[29] V. Galdi, L. Ippolito, a. Piccolo, and a. Vaccaro, "A genetic-based methodology for hybrid electric vehicles sizing," *Soft Computing*, vol. 5, pp. 451–457, Dec. 2001.

[30] A. Hasanzadeh, B. Asaei, and A. Emadi, "Optimum design of series hybrid electric buses by genetic algorithm," *Energy*, pp. 1465–1470, 2005.

[31] X. Wu, B. Cao, J. Wen, and Z. Wang, "Application of particle swarm optimization for component sizes in parallel hybrid electric vehicles," in *Congress on Evolutionary Computation, CEC*, pp. 2874–2878, IEEE, 2008.

[32] C. Desai, F. Berthold, and S. S. Williamson, "Optimal drivetrain component sizing for a plug-in hybrid electric transit bus using multi-objective genetic algorithm," in *EPEC - Electrical Power and Energy Conference: "Sustainable Energy for an Intelligent Grid"*, pp. 1–5, IEEE, 2010.

[33] C. Mi, B. Li, D. Buck, and N. Ota, "Advanced electro-thermal modeling of lithium-ion battery system for hybrid electric vehicle applications," in *VVPPC- Proceedings of the IEEE Vehicle Power and Propulsion Conference*, pp. 107–111, 2007.

[34] E. Vinot, R. Trigui, B. Jeanneret, J. Scordia, and F. Badin, "Hevs comparison and components sizing using dynamic programming," in *VPPC - Proceedings of the IEEE Vehicle Power and Propulsion Conference*, pp. 314–321, 2007.

[35] X. Liu, Y. Wu, and J. Duan, "Optimal sizing of a series hybrid electric vehicle using a hybrid genetic algorithm," in *Proceedings of the IEEE International Conference on Automation and Logistics, ICAL*, pp. 1125–1129, 2007.

[36] R. Fellini, N. Michelena, P. Papalambros, and M. Sasena, "Optimal design of automotive hybrid powertrain systems," *Proceedings First International Symposium On Environmentally Conscious Design and Inverse Manufacturing*, pp. 400–405, 1999.

[37] C. Mi, M. A. Masrur, and D. W. Gao, *Hybrid electric vehicles principles and applications with practical perspectives*. John Wiley Sons, Ltd, 2011.

[38] B. Zhang, Z. Chen, C. Mi, and Y. L. Murphey, "Multi-objective parameter optimization of a series hybrid electric vehicle using evolutionary algorithms," in *5th IEEE Vehicle Power and Propulsion Conference, VPPC '09*, pp. 921–925, 2009.

[39] R. A. Weinstock, P. T. Krein, R. A. White, and A. V. B. Pack, "Optimal sizing and selection of hybrid electric vehicle components," *Power Electronics Specialists Conference, PESC'93 Record., 24th Annual IEEE*, pp. 251–256, 1993.

[40] S. K. Shahi, G. G. Wang, L. An, E. Bibeau, and Z. Pirmoradi *Journal of Mechanical Design, Transactions Of the ASME*, no. 9.

[41] S. A. Rahman, N. Zhang, and J. Zhu, "Modeling and simulation of an energy management system for plug-in hybrid electric vehicles," in *Australasian Universities Power Engineering Conference, AUPEC*, 2008.

[42] "Argonne national laboratory." `http://www.anl.gov`.

[43] "Hybrid vehicle dismantling manual." `http://techinfo.toyota.com/techInfoPortal/staticcontent/en/techinfo/html/prelogin/docs/priusphvdisman.pdf`.

[44] N. Kim, A. Rousseau, and E. Rask, "Autonomie model validation with test data for 2010 Toyota Prius," *SAE Technical Papers*, 2012.

[45] N. Kim, S. Cha, and H. Peng, "Optimal control of hybrid electric vehicles based on pontryagin's minimum principle," *IEEE Transactions on Control Systems Technology*, vol. 19, pp. 1279–1287, Sept. 2011.

[46] A. Rousseau, "Included in autonomie. initialization file:ess-li-41-54-pngvanl-saftvl41m-pi-cstr.m."

[47] A. Rousseau, "Included in autonomie. initialization file:accelec-plant-300.m."

[48] F. Besnier, "Included in autonomie. initialization file:pc-plant-090-12.m."

[49] F. Bourry, "Included in autonomie. initialization file:pc-plant-boost-095.m."

[50] A. Taghavipour, N. L. Azad, and J. McPhee, "Design and evaluation of a predictive powertrain control system for a PHEV to improve fuel economy and emissions," *Journal of Automobile Engineering (under review)*, 2013.

[51] "Case study: Toyota hybrid synergy drive." `http://www.ae.pwr.wroc.pl/filez/20110606092430_HEV_Toyota.pdf`.

[52] "Toyota prius user-guide." `http://john1701a.com/prius/documents/Prius_User-Guide.pdf`.

[53] "Toyota website." `http://www.toyota.com`.

[54] S. Golbuff, "Optimization of a plug-in hybrid electric vehicle," Master's thesis, Georgia Institute of Technology, 2006.

[55] S. Chanda, *Powertrain Sizing and Energy Usage Adaptation Strategy for Plug-in Hybrid Electric Vehicles*. PhD thesis, University of Akron, 2008.

[56] "Toyota 0-60 times." `http://www.zeroto60times.com/Toyota-0-60-mph-Times.html`.

[57] A. Taghavipour, R. Masoudi, L. Azad, N, and J. McPhee, "High-fidelity modeling of power-split plug-in hybrid electric powertrains for control performance evaluation," *Proceedings of the ASME International Design Engineering Technical Conferences*, Aug. 2013.

[58] J. F. Kennedy, J. Kennedy, and R. C. Eberhart, *Swarm intelligence*. Morgan Kaufmann, 2001.

[59] M. Sniedovich, *Dynamic programming: Foundations and principles*. CRC press, 2010.

[60] M. Melanie, "An introduction to genetic algorithms," *Cambridge, Massachusetts London, England, Fifth printing*, vol. 3, 1999.

[61] R. Vijayagopal, J. Kwon, A. Rousseau, and P. Maloney, "Maximizing net present value of a series phev by optimizing battery size and vehicle control parameters," *SAE International Journal of Passenger Cars-Electronic and Electrical Systems*, vol. 3, no. 2, pp. 56–67, 2010.

[62] "Cost of power." `http://batteryuniversity.com/learn/article/cost_of_power`.

[63] "Gas price data." `http://www.gasbuddy.com/gb_retail_price_chart.aspx?time=24`.

[64] "Lithium battery prices still falling." `http://www.gavinshoebridge.com/batteries/hey-electric-car-fans-lithium-battery-prices-still-falling`.

[65] M. Ehsani, Y. Gao, and A. Emadi, *Modern electric, hybrid electric, and fuel cell vehicles: fundamentals, theory, and design*. CRC press, 2009.